# The influence of ammonia on the laminar burning velocities of methylcyclohexane and toluene: an experimental and kinetic modeling study

*Marco Lubrano Lavadera*[a]*, *Matteo Pelucchi*[b], *Alexander A. Konnov*[a]

[a]Division of Combustion Physics, Lund University, SE-22100 Lund, Sweden

[b]CRECK Modelling Lab, Department of Chemistry, Materials and Chemical Engineering "G. Natta", Politecnico di Milano, Milano, Italy

[*]**Corresponding author:**

Marco Lubrano Lavadera

Division of Combustion Physics,

Lund University,

P.O. Box 118, SE-22100

Lund, Sweden

Email: marco.lubrano_lavadera@forbrf.lth.se

**Abstract**

Laminar burning velocities of methylcyclohexane and toluene blended with ammonia have been determined using the heat flux method at atmospheric pressure and initial temperature of 338 K, over equivalence ratios ranging from 0.7 to 1.3 and ammonia blending fractions in the binary fuel mixtures from 0 to 90%. It was observed that the addition of ammonia to methylcyclohexane and toluene leads to a decrease in laminar burning velocity that is not proportional to the ammonia mole fraction. Such a burning velocity reduction is due to synergistic thermal and kinetic effects. In addition, ammonia has a slightly higher impact on the burning velocities of toluene due to fuel structure effects. The CRECK detailed kinetic model has been used to interpret the experimental measurements and minor modifications on methylcyclohexane, toluene, and methyl-phenoxy radical chemistry allowed even improved agreement. New experimental results have been compared with predictions of this refined kinetic mechanism. The model provided good predictions of the measurements capturing the effect of equivalence ratio and ammonia fraction ranges investigated. Finally, a mass fraction-based mixing rule was shown to be predictive for binary blends of $NH_3$ with methane and several hydrocarbons typically used to formulate surrogates for practical fuels.

**Keywords**: Ammonia; Laminar burning velocity; Methylcyclohexane; Toluene; Kinetic mechanism; Heat flux method.

## 1. Introduction

Recently ammonia ($NH_3$) has received revitalized interest as a promising renewable and carbon-free energy carrier. This consideration has motivated numerous test studies focused on direct $NH_3$ utilization in internal combustion engines, stationary gas turbines, and industrial furnaces as recently summarized by Valera-Medina et al. [1]. Such investigations mainly focused on overcoming the nitrogen-based pollutant emissions and the unfavorable combustion characteristics of $NH_3$ compared to conventional hydrocarbon fuels such as its low flame temperature, low laminar burning velocity, high auto-ignition temperature, narrow flammability range, high heat of vaporization, low lower heating value (on a mass basis), high minimum ignition energy, high ignition delay time, low radiation intensity, and slow chemical conversion rate.

In order to address these challenges, several investigators have considered enhancing the combustion by doping $NH_3$ with $H_2$ [2-16], which could be produced in situ from $NH_3$ partial dissociation, leading to better ignitability, increased laminar burning velocity and extended flammability range. Another potential combustion promoter that has been tested is methane, the main fuel for gas turbines power generation [7, 17-19]. Contemporary studies also extensively investigated the performances of dual fueled combustion of $NH_3$ with diesel [3, 20-23], biodiesel [20], and dimethyl ether [24, 25] in compression-ignition engines; gasoline [4, 6, 26-28] or gasoline/alcohols [29] in spark-ignition engines; and kerosene in gas turbines [19]. These co-firing approaches are of practical interest either to reduce carbon-based emissions, or to enhance combustion when $NH_3$ is the primary fuel.

Such studies have succeeded in demonstrating the potential of $NH_3$ as a flexible fuel in conventional combustion systems without major design modifications and, for this purpose, the relevance of auxiliary fuels to be co-fired with $NH_3$ to counteract its unfavorable combustion

properties has been underlined. However, despite the encouraging progress that has been reached in the implementation of $NH_3$ in current combustion-based applications, the optimal design and reliable operation of practical combustors over a wide range of conditions also require a thorough understanding of the combustion chemistry of $NH_3$-containing mixtures. While various chemical kinetic models have been proposed and validated for hydrocarbons and $NH_3$ individually, it is not the case for their blends. Such a gap between kinetic studies of neat fuels and engine studies of fuel mixtures emphasizes the need for fundamental experimental data of high fidelity on these blends to provide additional useful validation targets for a comprehensive model validation.

One of the key fundamental properties to characterize the combustion behavior of any fuel or fuel blend is the laminar burning velocity ($S_L$). Its knowledge is invaluable for the design of combustion devices, for turbulent combustion modeling, and for the validation of chemical reaction mechanisms. As a matter of fact, in an effort to advance this understanding, recent works by several research groups considerably extended the experimental $S_L$ database of $NH_3$-based mixtures [16, 30-47]. The availability of these target data boosted the development of new detailed kinetic mechanisms that provided important insights into the underlying oxidation process of $NH_3$ and its blends with hydrogen, syngas, and natural gas. Nevertheless, the information available in archival literature is still insufficient considering that, to the best of our knowledge, dedicated studies focused on the interactions of $NH_3$ with practical hydrocarbon fuels, such as gasoline, diesel, or kerosene, are only limited to our recent publication [48], where $S_L$ for blends of n-heptane, iso-octane, and methane with $NH_3$ were experimentally and numerically explored and the results interpreted on the basis of thermal, kinetic and transport effects. It was shown that the influence of $NH_3$ on the high-temperature combustion behavior of high-molecular-weight fuels is quite general because the co-oxidation of $NH_3$ and large-carbon-number hydrocarbons occurs with little mutual

interaction and the controlling role is held by the oxidation rates of small fragments in the main reaction zone of the flame, similar to $NH_3$-$CH_4$ systems. However, it is not certain whether this is also true for flames of $NH_3$ in combination with other reference fuel classes typically present in real transportation fuels, such as aromatics and naphtenes, where the fuel-specific intermediate distribution plays a more important role compared to n- and iso-paraffins. Additional experiments and analyses can answer this question, which is the goal of the present work. Therefore, two essential components of any road or jet engine fuel surrogate [49, 50], namely methylcyclohexane (MCH) and toluene, are selected in this study as the representatives of cycloparaffins and aromatics. The specific objective is to measure the $S_L$ of their blends with $NH_3$ over a broad stoichiometry range using the heat flux method to comparatively examine the effect of $NH_3$ enrichment on flame propagation in the case of hydrocarbons with the same carbon atom number (i.e., C7) but different molecular structures. Furthermore, the results are interpreted in terms of a chemical kinetic model presented and minorly updated for the scopes of this work.

## 2. Experimental details

Premixed laminar flames were stabilized at atmospheric pressure on a flat flame burner compliant with the heat flux method. The stationary flames generated through this method can essentially be considered adiabatic, one-dimensional, and stretchless. A detailed description of the method, experimental setup, operation, data processing, and uncertainty analysis can be found elsewhere [51], thus only the key elements are outlined here.

All heat flux burners employed so far in our laboratory are made of brass and it is well known that $NH_3$ can be corrosive towards such a material. Hence, the burner with the worst performances due to an old design, designated as burner “E2” by Alekseev et al. [51], was employed. This burner

was already successfully used for measuring $S_L$ of $NH_3$-containing mixtures [47, 48] where the influence of $NH_3$ adsorption on the brass surface was considered to be negligible. However, its use leads to a higher uncertainty of the measured $S_L$ than commonly reported for measurements performed with the heat flux method (usually < 1 cm/s) [48].

The burner plate and the plenum chamber were both heated using circulating water throughout two separate jackets. During the experiments, the temperature of the plate edge was maintained at 368 K, while the temperature of the plenum chamber at 338 K (± 1 K). The latter fixes the desired initial temperature of the fresh gas mixture ($T_g$). This temperature was chosen in order to cover a wide range of equivalence ratios, which is constrained by the vaporization limit of the mixtures.

The positive temperature difference between the burner plate and the inlet mixture allows compensating the heat loss necessary for stabilizing the flame and the heat gain of the unburned gas from the plate. When the two terms are balanced, the net heat flux is zero and an adiabatic flame with respect to the burner is created. For this condition, the radial temperature distribution over the burner plate is uniform and equal to the temperature of the burner plate. This is recorded by eight Chromel-Constantan shielded thermocouples, whose junctions (0.5 mm diameter) are inserted into different holes of the burner surface at specific radii from the center. By changing the flow rate of the fresh gas mixture, an appropriate value can be found to achieve such a condition, where the velocity of the unburned gas corresponds to $S_L$. Hermanns [52] found that the temperature difference between the burner plate and $T_g$ should be higher than 30 K to avoid flame instabilities. However, as explained, this $\Delta T$ has been set to 30 K in the present experiments. Consequently, most of the investigated flames exhibited corrugation or cellularity around adiabatic conditions. In these cases, $S_L$ was determined by extrapolation from flat sub-adiabatic conditions.

An example of evaluating $S_L$ from sub-adiabatic flames and the associated uncertainties can be found in [51].

A mixing panel provides controlled flow rates and compositions of the fresh mixtures. The liquid fuels feeding system consists of a stainless steel reservoir pressurized with nitrogen to feed the fuel through a Coriolis liquid mass flow controller into a Controlled Evaporator Mixer (CEM), both from Bronkhorst High-Tech. The total uncertainty of the liquid flow rate is a sum of 0.5 g/h plus the stated flow repeatability of the liquid flow controller, which is within 0.2% of the set-point. Neat MCH and toluene were used as delivered respectively by Alfa Aesar and Merck in sealed bottles and their purity was ≥ 99%. The gases, $NH_3$ (99.98%) and synthetic air (21% $O_2$, 1% relative uncertainty), were delivered by AGA and their required flow rates were controlled through two Bronkhorst High-Tech digital thermal mass flow controllers. The air flow was also used as a carrier gas to facilitate the vaporization process as a mixing component and to transport the vapor. The two gas flow controllers were calibrated shortly before the measurements using a positive displacement calibrator (MesaLabs Definer 220). The total uncertainty of the gas flow rates is a sum of 1% stated accuracy of the calibrator plus the stated flow repeatability of the mass flow controllers, which corresponds to 0.2% of the set operating conditions. To prevent fuel condensation throughout the fueling system, an electrically heated pipe was used to connect the evaporator to the plenum chamber and its temperature was set equal to $T_g$.

Detailed analysis and quantification of the experimental uncertainties were reported earlier [51] and the relative combined standard uncertainty of $S_L$ in the present measurements was estimated to be between 4.4 and 6.4%, depending on the experimental conditions. Measurements were conducted for single-component MCH/air and toluene/air mixtures and binary blends of them with $NH_3$. For the blends, two volume contents of $NH_3$ were considered, namely 0.25 and 0.50, with a

maximum combined standard uncertainty in the $NH_3$ mole fraction of 0.006. For these mixtures, the equivalence ratio (Φ) was adjusted from 0.7 to 1.3 with uncertainty between 0.013 and 0.021. Then, in stoichiometric mixtures, the mole fraction of $NH_3$ was varied from 0 to 0.9 with a step of 0.1. Due to the very low reactivity of $NH_3$, it was not possible to increase its mole fraction above 0.9 with the present installation. In particular, when the $S_L$ falls below about 10 cm/s, which is the case of pure $NH_3$, stabilization of the flame on a heat flux burner is only possible by increasing the difference between the temperature of the burner plate and $T_g$ to values higher than 70 K, for example using oil instead of water as the heating fluid [41]. The experimental values of the $S_L$ measured in the present study with the associated uncertainties are given in the Supplementary Material (Tables S1-S8).

## 3. Modeling details

Numerical simulations were performed by solving the one-dimensional, freely propagating, adiabatic flame problem with the Premixed Laminar Flame-Speed module of the ANSYS Chemkin 17.0 software. The steady-state mass, species, and energy conservation equations were solved with non-uniform mesh spacing, using a mixture-averaged transport formula, without radiative heat transfer and including thermal diffusion. A grid-independent solution was ensured by setting the parameters GRAD and CURV to 0.03, resulting in a number of grid points around 500-700 over the domain of 3 cm. This numerical tool was used to compute $S_L$ and to perform kinetic analyses to study the effect of $NH_3$ concentration on the propagation of MCH/$NH_3$ and toluene/$NH_3$ mixtures.

To the best of our knowledge, the CRECK model is the only one suitable for predicting $S_L$ in flames of $NH_3$ and hydrocarbons with chain lengths above $C_3$. Moreover, it has been shown that

this model accurately captures the $S_L$ of methane, n-heptane, iso-octane, and their blends with $NH_3$ [48]. Thus, it is meaningful to validate and expand its application range to blends of MCH and toluene with $NH_3$, which has never been done before owing to the lack of validation data.

### 3.1 Kinetic model

The CRECK kinetic model (2003, March 2020) [53] developed at Politecnico di Milano accounts for the combustion chemistry of a variety of species relevant to gasoline, bio-fuels and bio-oils, diesel, bio-diesel and aviation fuels [54]. The modular structure of the CRECK model allows to seamlessly couple additional modules such as $NO_x$ [55] and $NH_3$ chemistry [56], as well as a discrete sectional soot formation model, also developed at CRECK [57-59]. The model thus obtained constitutes a suitable tool also for the analysis of compositional effects on the formation of pollutants.

At the core of the kinetic model is the Aramco C0–C2 mechanism from Metcalfe et al. [60] and the C3 subset from Burke et al. [61]. Updates from [62] have been recently reported for the C0–C1 chemistry. A discussion of the low- and high-temperature combustion mechanisms and of the general principles used to represent heavier components can be found in Ranzi et al. [54]. Recent updates to mono-aromatic and poly-aromatic hydrocarbons are reported in [63-66]. Specifically, the MCH and toluene subsets are respectively from Mairinger et al. [67] and from Pelucchi et al. [68]. Some minor modifications to the MCH and toluene subsets have been applied so as to better match the new experimental data presented in this work, as discussed in Section 3.2. A wide range of validation of the updated model is reported in the Supplementary Material (Figs. S1-S33) and includes speciation data in different ideal reactors as well as ignition delay times in shock tubes and rapid compression machines and other laminar burning velocity measurements [69-93]. The

objective of such effort is to always guarantee the best compromise between performances over a wide range of experimental conditions (T, p, Φ, and fuels or fuel mixtures) and new theoretical findings, or experimental evidences [94].

The kinetic model thus obtained is provided, with thermodynamic and transport properties, as Supplementary Material to this study. The high temperature mechanism that we suggest for flame simulations contains 396 species and 12819 reactions, including $NH_3/NO_x$ subset [55, 56]. The global high and low temperature mechanism, covering both the high and low temperature oxidation regimes for MCH, toluene and other reference fuels contains 520 species and 15924 reactions and is also attached for sake of completeness.

### 3.2 Modifications to the original CRECK kinetic model

Table 1 shows reactions belonging to MCH and toluene subsets for which rate constants have been modified for the purposes of this study, with respect to the original CRECK mechanism (March 2020, version 2003) [64, 67, 68]. Figure 1 shows comparisons between rate constants from the previous CRECK mechanism and from the literature. The full set of validation targets, covering both high and low temperature oxidation conditions is reported in the Supplementary Material. Table 1 also reports the references to the specific studies from which the rate constants have been adopted, detailing the extent of the adjustments compared to the starting CRECK kinetic model. Most of the modifications deal with the production or consumption of Ḣ. Indeed, as discussed by Ranzi et al. [95], reactions producing Ḣ such as radical decomposition reactions, initiation reactions breaking a C-H bond generally increase $S_L$, as they provide Ḣ atoms to the branching reaction dominating the chemistry of flames, i.e. $\dot{H}+O_2=\dot{O}H+\ddot{O}$. Conversely, reactions consuming Ḣ such as H-abstraction and recombination reactions inhibit flame propagation. This can be clearly

seen from Fig. 2, which reports the first order normalized sensitivity of $S_L$ for stoichiometric MCH/air and toluene/air flames computed using the CRECK original mechanism.

**Table 1**: Rate constants modified in the context of this work. Units are $cm^3$, mol, s, cal.

| | Reaction | A | n | Ea [cal/mol] | Reference \| Notes |
|---|---|---|---|---|---|
| **R1** | $\dot{H}+MCYC6 \leftrightarrow H_2+RMCYC6$ | $6.74\ 10^6$ | 2.46 | 5238.05 | [96] \| A x 2 [a] |
| **R2** | $\dot{H}+C_7H_8 \leftrightarrow C_7H_7+H_2$ | $1.07\ 10^6$ | 2.27 | 4392.37 | [97] \| A / 2 [b] |
| **R3** | $\dot{H}+C_7H_8 \leftrightarrow CH_3C_6H_4+H_2$ | $2.00\ 10^8$ | 1.83 | 14381.82 | [97] \| A / 2 [b] |
| **R4** | $RCRESOL\dot{O} \rightarrow C_6H_6+\dot{H}+CO$ | $9.00\ 10^{13}$ | 0.00 | 52000.00 | [64, 68] \| A x 1.5 [b, c] |
| **R5** | $\dot{H}+RCRESOL\dot{O} \leftrightarrow CRESOL$ | $1.00\ 10^{14}$ | 0.00 | 0.00 | [64, 68] \| A / 1.5 [b, c] |
| **$R5_{rev}$** | | $8.90\ 10^{14}$ | 0.00 | 85864.98 | [64, 68] \| A / 1.5 [b, c] |

*Notes: [a] modification since Mairinger et al. [67], [b] modification since Pelucchi et al. [68], [c] modification since Pelucchi et al. [64].*

*R4 and R5 are high pressure limit rate constants.*

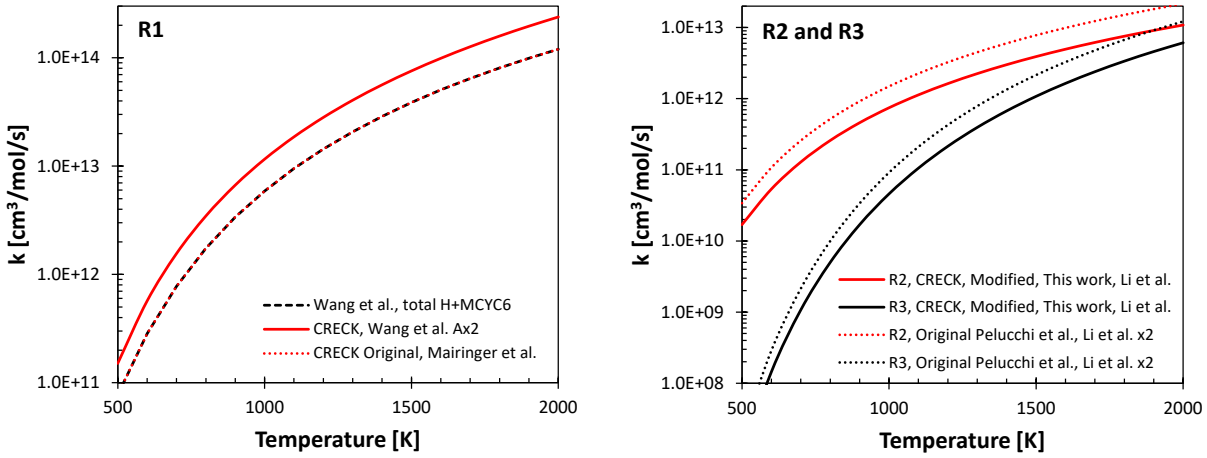

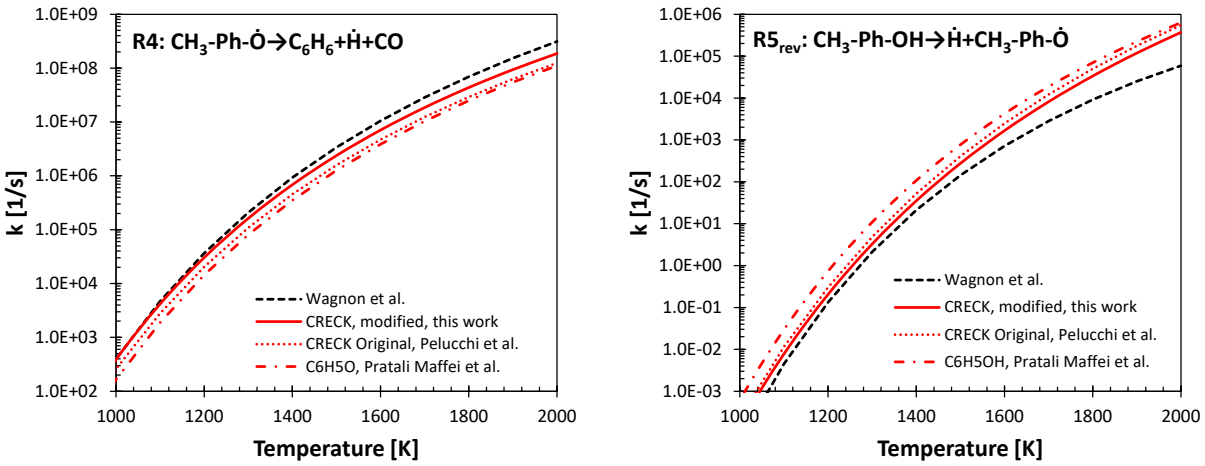


**Figure 1**. Comparisons between rate constants from the CRECK original mechanism [64, 67, 68] and rate constants in the modified mechanism here presented. Literature values of the same or analogous reactions (e.g. phenol/phenoxy) are also reported [66, 98].

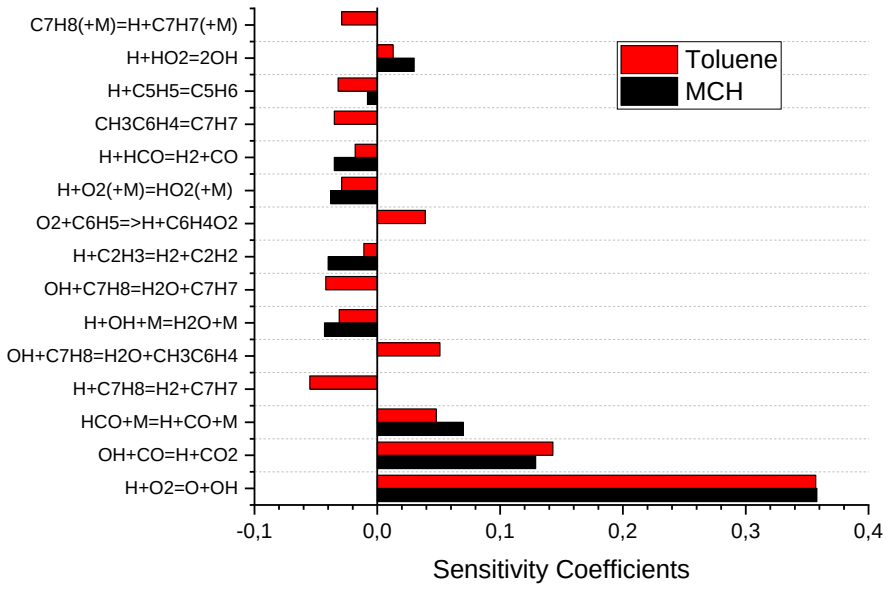


**Figure 2**. $S_L$ sensitivity coefficients calculated for stoichiometric MCH-air (black bars) and toluene-air (red bars) mixtures at 1 atm and 338 K using the CRECK original mechanism.

Rate coefficients have been modified by a maximum factor of 2, which is well within the uncertainties of theoretical studies, where available, and well below expected uncertainties for rate constants derived by analogy or less accurate estimates. H-abstraction reactions by Ḣ from MCH (denoted in the model as MCYC6) have been theoretically determined by Wang et al. [96] using CBS-QB3. Uncertainties in single point energies calculations with CBS-QB3 are in the order of ~2.5 kcal/mol as reported by Simmie and Somers [99]. This uncertainty in energy barriers already reflects into a factor of ~1.9-3.5 over the temperature range T=1000-2000 K, even neglecting uncertainties in frequencies, and therefore partition functions, determination. The rate constants proposed by Wang et al. [96] were originally adopted as reported in Mairinger et al. [67] and increased by a factor of 2 in this study for (R1). Li et al. [97] theoretically investigated the H-abstraction reactions by Ḣ from toluene (denoted in the model as $C_7H_8$) (R2 and R3) using the G4 method that provides a slightly improved accuracy (~1 kcal/mol) compared to CBS-QB3 [99]. For this reason, rate constants by Li et al. [97] were increased by a factor of 2 in the work of Pelucchi et al. [68] on toluene pyrolysis and oxidation. In this study, we have chosen to adopt the original values by Li et al. [97] to further improve the agreement with the new $S_L$ measurements presented in this study without significantly affecting other validation targets.

Methyl-phenol (CRESOL, CH3-Ph-OH where Ph represents the aromatic ring) and methyl-phenoxy radical (CH3-Ph-Ȯ) play a key role in toluene oxidation kinetics as deeply discussed previously [68, 100]. Resonantly stabilized methyl-phenoxy radical (RCRESOLȮ) is formed by the addition of methyl-phenyl radical to $O_2$ ($O_2$+$CH_3C_6H_4$↔RCRESOLȮ+Ö) as discussed by da Silva et al. [100]. Successive reactivity of methyl-phenoxy radical in flames can lead to termination, when recombination with Ḣ occurs (R5), or branching through a decomposition reaction (R4), analogous to phenoxy radical decomposition to cyclopentadienyl radical ($C_5H_5$) and

CO recently investigated in [66]. R4 is implemented in a lumped form so as to avoid the inclusion of α-hydrofulvenyl radical. Based on the sensitivity analysis we decreased by a factor of 1.5 the termination channel (R5) and increased by the same amount the branching channel (R4). Our final values fall well within an average factor of ~3 from the recent theoretical determination of $C_6H_5\dot{O}+H\leftrightarrow C_6H_5OH$ and $C_6H_5\dot{O}\leftrightarrow C_5H_5+CO$ by Pratali Maffei et al. [66], and within a factor of ~2-5 from the estimates by Wagnon et al. [98]. Overall, it is our belief that such modifications to cresol chemistry are generally within expected uncertainties of available rate constants from the literature. However, systematic theoretical studies for such reaction classes (i.e. radical recombination reactions, unimolecular initiation reactions, addition to $O_2$ of phenyl-like radicals, etc.) should be performed for aromatic and oxygenated aromatic compounds such as benzene, toluene, phenol and phenolic species with multiple substitutions, along the same lines of recent theoretical investigations [65, 66].

## 4. Results

### 4.1 Validation of the experimental and modeling methodology

First, to assess the accuracy of the present measurements, a comparison with benchmark $S_L$ data available in the literature for pure MCH and toluene is carried out and it is presented in Figs. 3 and 4 at an initial temperature of 338 K and atmospheric pressure, over a Φ range of 0.7-1.3. There have been several determinations of $S_L$ for the aforementioned fuels, though only two studies have been conducted at the same initial conditions as the present work. In particular, the $S_L$ for MCH have been reported by Matveev et al. [101], while the $S_L$ for toluene have been provided by Sileghem et al. [102]. Similar to the data from this study, both the literature data sets have been obtained using the heat flux method, but in different laboratories.

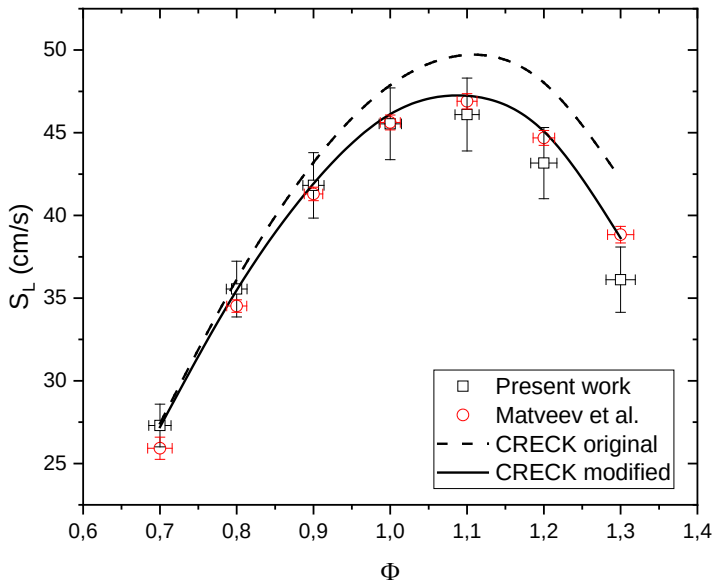


**Figure 3.** Experimental (symbols) and simulated (lines) $S_L$ of MCH-air flames versus Φ at $T_g$=338 K and p=1 atm. Black squares: present work. Red circles: Matveev et al. [101]. Dashed line: CRECK original. Solid line: CRECK modified.

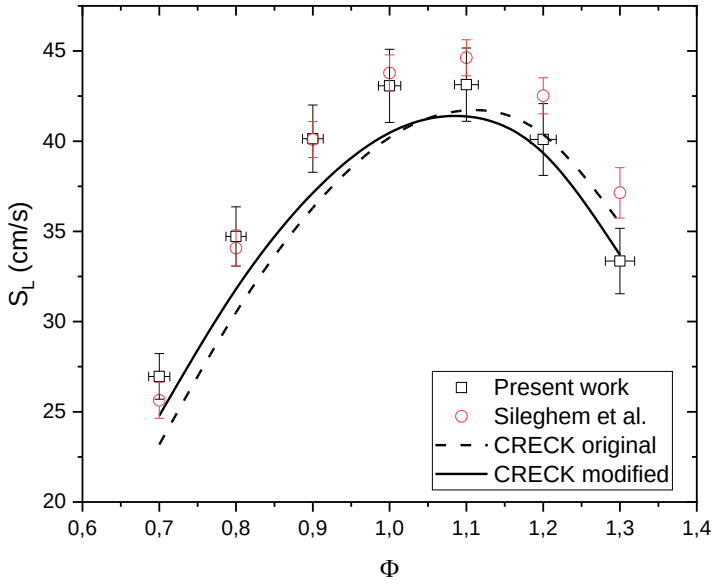


**Figure 4.** Experimental (symbols) and simulated (lines) $S_L$ of toluene-air flames versus Φ at $T_g$=338 K and p=1 atm. Black squares: present work. Red circles: Sileghem et al. [102]

(corrected according to re-evaluation reported in [51]). Dashed line: CRECK original. Solid line: CRECK modified.

A classical evolution as a function of Φ, with the peak value of $S_L$ at Φ=1.1 is obtained for both fuels. It can be seen from Figs. 3 and 4 that MCH-air mixtures exhibit higher $S_L$ than toluene-air mixtures throughout the whole range of Φ, which is consistent with earlier literature reports [103, 104].

The experimental data measured in the current work are found in very good qualitative and quantitative agreement with those obtained before in other studies, especially for Φ < 1.1. This confirms the reproducibility of the heat flux experiments within the evaluated uncertainties and gives confidence in the experimental set-up and the measurements performed herein for reliable validation of kinetic models. However, it should be noted that for both fuels the agreement deteriorates in the case of rich mixtures where the present $S_L$ are slightly lower compared to the previous measurements and, at Φ=1.3, the experimental data do not overlap within the evaluated uncertainties. Before validating the kinetic model using these data, one must examine the possible factors which may cause these differences for rich flames. A similar systematic shift on the fuel-rich side with the burner used in this work was already observed in [48] in the case of pure n-heptane and iso-octane. It was suggested that instabilities manifested as cellular flames are the reason for the observed discrepancy under rich conditions. In particular, in the previous studies reported in Figs. 3 and 4 [101, 102], cell formation was observed at Φ > 1.3, in contrast to our previous [48] and current measurements where such instabilities were also observed at lower Φ. It can be inferred that the burner used in the present work, due to the old design, produces less accurate $S_L$ data in the fuel-rich region when liquid fuels are tested, but a maximum discrepancy

of about 3 cm/s at Φ = 1.3 is anyhow considered acceptable to extract fundamental information from these data.

In addition, the above data were adopted to evaluate the performance of the proposed model. Thus, the computed $S_L$ are shown in Figs. 3 and 4 together with the corresponding experimental data. Simulations for pure MCH and toluene were performed using the original CRECK and the model updated in the present work, named as CRECK modified. As shown in Figs. 3 and 4, the chemical kinetic simulations with both the original and the modified CRECK models confirm the general shape of the $S_L$ data and predict the peak at around Φ=1.1, which is consistent with the experimental data.

Regarding MCH (Fig. 3), the comparison demonstrates that the $S_L$ are largely better predicted by the modified CRECK over the entire Φ range. In particular, the modifications illustrated in Table 1 lead to a decrease in $S_L$ of 0.2 cm/s at Φ=0.7, 2.5 cm/s at Φ=1.1, and 3.6 cm/s at Φ=1.3 respectively.

Regarding toluene (Fig. 4), it is seen that the modifications adopted in the kinetic mechanism yield an increase of the predicted $S_L$ under lean conditions (1.6 cm/s at Φ=0.7) and a decrease under rich conditions (1.8 cm/s at Φ=1.3). The $S_L$ computed for the fuel-rich mixtures with the refined mechanism are somewhat lower than the data of [102], but they agree quite well with the present experimental data. Despite the improvement of the predictions on the lean side, the $S_L$ are still underpredicted for Φ below 1.1, but the discrepancy between the experimental data and the modified CRECK is smaller compared to the original version. Moreover, the shape of the evolution of the $S_L$ with Φ seems to be better captured by the modified model.

Therefore, while noticeably good agreement between experimental and computed MCH data can be reached as shown in Fig. 3, Fig. 4 indicates that the toluene oxidation mechanism may need

further improvement. This requires additional systematic theoretical studies for reaction classes concerning oxygenated aromatic intermediates, as already discussed in Section 3.2. However, the overall improvement observed on the basis of the comparative experimental and computed results, without deterioration of the predictive performances against other targets (see Supplementary Material) also including other $S_L$ measurements [85, 86, 92, 93, 102, 103], proves that the modified CRECK model is applicable for the present study. Thus, it was adopted for the following analysis.

### 4.2 Influence of $NH_3$

In the present section, first, the $S_L$ results for pure MCH and toluene, as well as their binary blends with 25% (± 0.4%) and 50% (± 0.6%) of $NH_3$, are presented for the same Φ range (0.7-1.3). Next, effects of the addition of up to 90% (± 0.4%) of $NH_3$ on MCH and toluene are systematically investigated at Φ=1. All the experiments were carried out at initial conditions of 338 K and 1 atm.

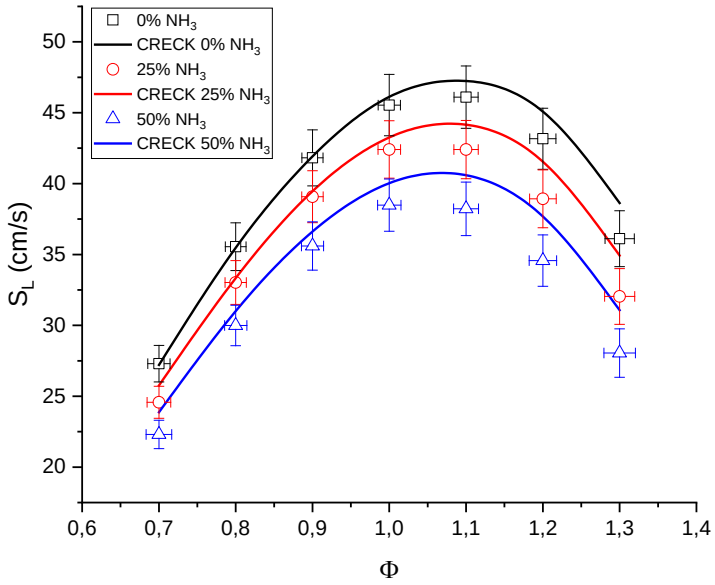

**Figure 5.** Experimental (symbols) and simulated (lines) $S_L$ of MCH/$NH_3$-air flames versus Φ at $T_g$=338 K and p=1 atm. Black squares and solid line: $NH_3$ mole fraction=0. Red circles and solid line: $NH_3$ mole fraction=0.25. Blue triangles and solid line: $NH_3$ mole fraction=0.5.

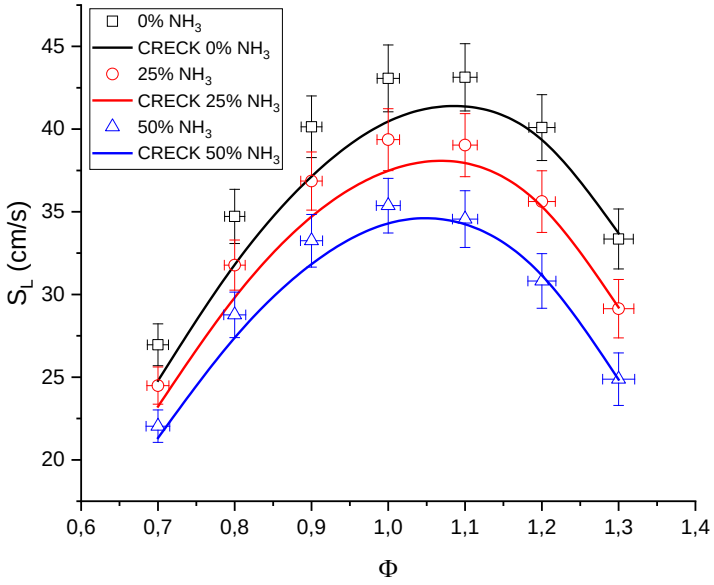


**Figure 6.** Experimental (symbols) and simulated (lines) $S_L$ of toluene/$NH_3$-air flames versus Φ at $T_g$=338 K and p=1 atm. Black squares and solid line: $NH_3$ mole fraction=0. Red circles and solid line: $NH_3$ mole fraction=0.25. Blue triangles and solid line: $NH_3$ mole fraction=0.5.

$S_L$ measured for the blends are shown in Figs. 5 (MCH/$NH_3$) and 6 (toluene/$NH_3$) for the same initial conditions. The results illustrate that $NH_3$ addition to the fuels causes a decrease of $S_L$ over the entire range of Φ as expected and that the peak $S_L$ shifts towards the stoichiometric mixture for increasing amounts of $NH_3$ concentration in the blends. The peak $S_L$ for pure MCH and toluene is 46 and 43.1 cm/s respectively; at 25% $NH_3$, it is 42.4 and 39.4 cm/s, while at 50% $NH_3$ it is 38.5 and 35.4 cm/s. This suggests that the addition of $NH_3$ has a similar effect on MCH and toluene. Moreover, it can be seen from Figs. 5 and 6 that, with the increase of $NH_3$ volume fraction, the

percentage decrease in $S_L$ is slightly higher under rich conditions. Similar observations were reported in [48] for $NH_3$/n-heptane and $NH_3$/iso-octane mixtures.

Along with the measured $S_L$ plotted against Φ, Figs. 5 and 6 also show the results of one-dimensional simulations using the present updated CRECK mechanism. The calculated values reasonably agree with the experimental data within the limits of experimental uncertainty, with a slight overprediction under rich conditions for MCH/$NH_3$ blends and a slight underprediction under lean conditions for toluene/$NH_3$ blends, regardless of the value of the $NH_3$ mole fraction. It is clear that the discrepancy in the case of toluene/$NH_3$ blends originates from the underprediction of the $S_L$ for neat toluene, as already discussed in the previous section. On the other hand, the small discrepancy in the case of MCH/$NH_3$ blends is consistent with the analysis presented in Fig. 3, where the present experimental values were shown to be lower than the reference literature data at $\Phi > 1.1$. Despite this, the elucidation of $NH_3$ enrichment effects, which is the primary purpose of this study, is not affected by these differences and it can be concluded that the current mechanism accurately captures the $S_L$ variation with $NH_3$ addition.

In order to more clearly examine the effect of $NH_3$ addition on $S_L$ of MCH and toluene, the $NH_3$ mole fraction in the binary blends was increased up to 0.9 with a step of 0.1 considering the stoichiometric mixture as a reference. Measured and predicted values of the $S_L$ of stoichiometric mixtures were normalized with respect to the $S_L$ of pure hydrocarbons ($S_L^0$) and the results are plotted in Fig. 7 as a function of the $NH_3$ quantity in the binary fuel mixtures. It was not possible to cover higher $NH_3$ ratios experimentally, as explained in Section 2. Therefore, $S_L$ obtained by Han et al. [41] for pure $NH_3$ is also plotted for comparison and is found to be consistent with the trend of the present results. Results show that from pure MCH or toluene to pure $NH_3$, $S_L$ decreases nonlinearly with the increase of $NH_3$ mole fraction in the fuel blend over the entire composition

range. Therefore, any mixing rule to be developed or identified would not be a simple mole fraction-based weighted average of the neat constituents $S_L$. For example, with the addition of 50% $NH_3$, the $S_L$ is reduced by only 15% from pure MCH and 18% from the pure toluene case. While at 90% of $NH_3$, the $S_L$ is decreased by nearly 48 and 51% from the two baseline conditions. As such, the effect of $NH_3$ in decreasing $S_L$ seems to be slightly more pronounced for toluene than for MCH under the tested conditions.

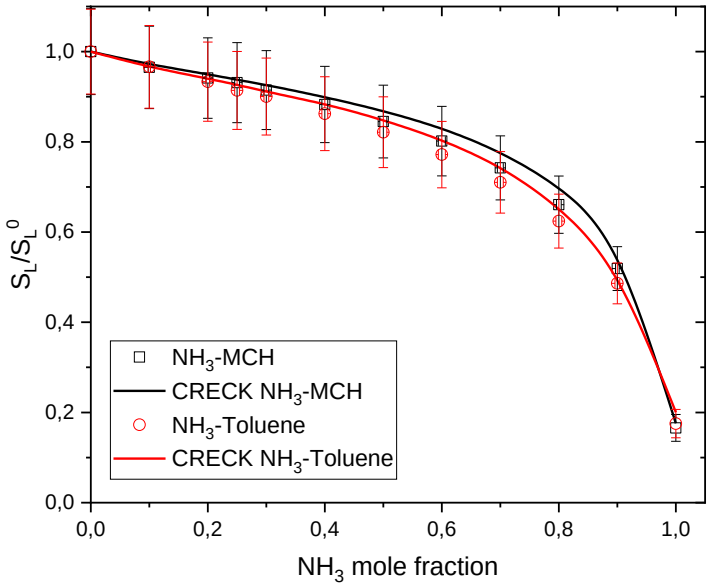


**Figure 7.** Experimental (symbols) and simulated (lines) stoichiometric $S_L$ ($\Phi$=1) versus $NH_3$ mole fraction at $T_g$=338 K and p=1 atm, normalized by $S_L$ of pure fuel/air mixtures ($S_L^0$). Black squares and solid line: MCH/$NH_3$-air mixtures. Red circles and solid line: toluene/$NH_3$-air mixtures. The value of $S_L$ for pure $NH_3$ is from [41].

Although in Fig. 6 the kinetic mechanism was shown to slightly underpredict the stoichiometric $S_L$ of toluene/air mixtures, the computed normalized profiles capture very well the monotonically decreasing trend of $S_L$ as a function of $NH_3$ percentage for both fuels. Furthermore, the nonlinear

evolution with $NH_3$ addition, as well as the relative difference between the two data sets observed experimentally, are confirmed. This means that the underlying mechanism responsible for the observed effect of $NH_3$ on the $S_L$ of MCH and toluene is accounted for in the kinetic model and it is unraveled in the next section.

## 5 Discussion

### 5.1 Numerical analysis

For the challenge of implementing $NH_3$ in current combustion-based applications, the variability and dependence of key characteristics such as the $S_L$ on $NH_3$ concentration in the fuel blends must be understood. In [48], it was found that the propagation process of $NH_3$-hydrocarbons laminar flames appears to be governed by two dominant synergistic factors dependent on the $NH_3$ concentration in the fuel blend: 1) the decrease of the adiabatic flame temperature ($T_{ad}$) as a result of the low energy content of $NH_3$ (thermal effect) and 2) the chemical inhibition of the overall reactivity caused by the radical scavenging of $NH_3$ (chemical effect). Therefore, before making any detailed analysis on the molecular structure effects, these two general features of the systems involved shall be verified. To do so, further numerical simulations have been carried out to separate these contributions. In particular, a fictitious species ($H_3N$) with identical molecular structure, transport, and thermodynamic properties to $NH_3$ has been defined. This virtual species however does not appear in the elementary reactions of the kinetic mechanism, and thus, it acts as a diluent. Then, simulations have been performed by numerically making the $T_{ad}$ of $H_3N$/hydrocarbons mixtures equal to that of $NH_3$/hydrocarbons mixtures in the range explored experimentally for the various fuels at $\Phi$=1, by modifying the $H_3N$ dilution, without altering the transport properties of the reacting mixtures. The sensitivity of $S_L$ to the decrease of $T_{ad}$ has been evaluated case by case with respect to the pure fuels as a reference by comparing the computed data. The results are

reported in Fig. 8, where the ordinate axis indicates the predicted values of the $S_L$ of stoichiometric mixtures normalized with respect to the $S_L$ of pure hydrocarbons ($S_L^0$) similar to Fig. 7 and the abscissa axis indicates the decrease of $T_{ad}$ ($T_{ad}^0$-$T_{ad}$). The solid lines represent the variations of $S_L$ that have been obtained for hydrocarbon/$NH_3$ mixtures, and the dashed lines represent the variations of $S_L$ that have been obtained for hydrocarbon/$H_3N$ mixtures. In other words, the difference between dashed lines and the pure hydrocarbons primarily reflects the thermal effects, while the difference between solid and dashed lines isolates purely kinetic effects.

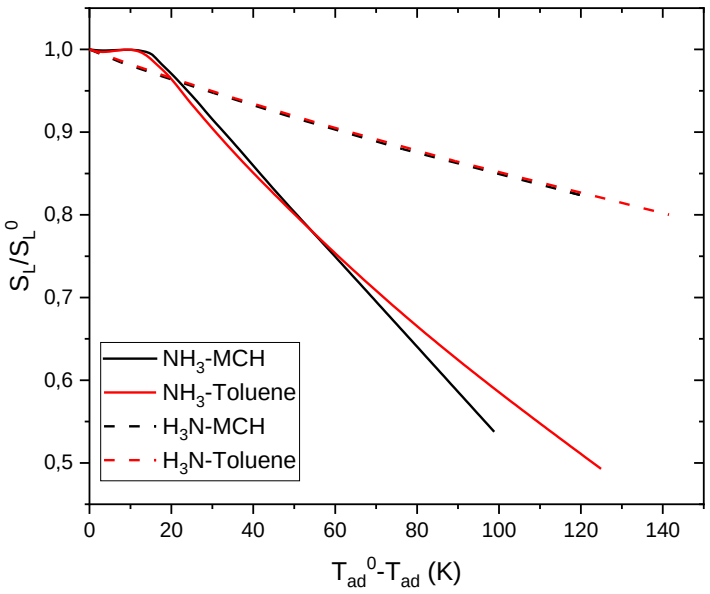


**Figure 8.** Simulated stoichiometric $S_L$ normalized by $S_L$ of pure fuel/air mixtures ($S_L^0$) at $T_g$=338 K and p=1 atm versus $T_{ad}^0$-$T_{ad}$ when blending the fuels with $NH_3$ (solid lines) and $H_3N$ (dashed lines). Black lines: MCH mixtures. Red lines: toluene mixtures.

These computational tests show that the thermal and chemical effects caused by $NH_3$ addition both contribute to the reduction of $S_L$. In detail, for a $T_{ad}$ decrease lower than 20 K, which corresponds to low $NH_3$ addition ratios (<10%), there is no global effect of $NH_3$ on $S_L$ (solid lines) but the

thermal effect (dashed lines) diminishes $S_L$ by about 3%. It means that the negative thermal effect is counterbalanced by a positive kinetic effect, that instead increases $S_L$. It was observed in [48] that the promoting effect of $NH_3$ addition on $S_L$ of heavy hydrocarbons is due to an increase in the hydrogen concentration in the flame zone. This was considered as a combined kinetic and transport effect because of the high reactivity and diffusivity of hydrogen. Then, for a constant $T_{ad}$ decrease of about 20 K, which corresponds to an $NH_3$ addition ratio of ~10%, the thermal effect plays the dominant role as the solid and dashed lines cross. The chemical effect increases with rising $NH_3$ blending ratios. For a $T_{ad}$ decrease between 35 and 40 K, which corresponds to $NH_3$ concentrations of about 40-50%, the chemical and thermal effects become comparable. For higher $NH_3$ ratios, the chemical effect is the main reason for the $S_L$ reduction and, for a $T_{ad}$ reduction higher than 60 K, which corresponds to $NH_3$ fractions higher than 70%, the ratio chemical/thermal effect is slightly more pronounced for the MCH/$NH_3$ mixtures. It is interesting to note that the high nonlinearity of the $S_L$ decrease with the increase of $NH_3$ fraction in the fuel blend observed in Fig. 7 mainly occurs when the chemical effect becomes dominant.

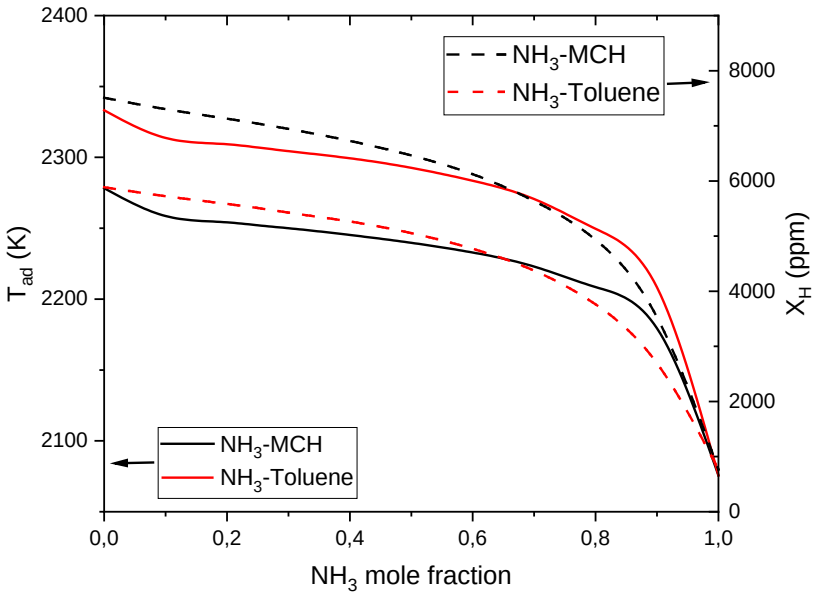

**Figure 9.** Simulated stoichiometric $T_{ad}$ (solid lines) and peak $X_H$ (dashed lines) versus $NH_3$ mole fraction at $T_g$=338 K and p=1 atm. Black lines: MCH/$NH_3$-air mixtures. Red lines: toluene/$NH_3$-air mixtures.

To gain more insight into these effects, Fig. 9 shows the impact of $NH_3$ fraction in fuel blends on the calculated $T_{ad}$ (left axis) and peak mole fraction of Ḣ radicals in the reaction zone ($X_H$, right axis) for the stoichiometric case using the present model. $T_{ad}$ represents the thermal effect on $S_L$, while $X_H$ reflects the effect of chemical kinetics. The analysis in Fig. 9 has been limited only to the Ḣ radical because, as discussed in Section 3.2, its generation and consumption reactions play a key role in accelerating and suppressing flame propagation. However, a similar result would have been obtained by showing the peak mole fraction of ȮH radicals. As expected, both $T_{ad}$ and $X_H$ significantly decrease as the $NH_3$ content in fuel blends increases and the profiles for both fuels have similar tendencies, which closely follow the variation of $S_L$ as a function of the composition of the fuel blends shown in Fig. 7. Figure 9 further shows that the $T_{ad}$ of the MCH/air flame is somewhat lower than that of the toluene/air flame by approximately 55 K due to the different C/H ratio, which is opposite to their $S_L$ order. On the other hand, it can be seen that the $X_H$ of the MCH/air is higher than that of the toluene/air flame by about 1600 ppm, which is consistent with their $S_L$ order. In fact, the $S_L$ of toluene is known [95] to be lower due to the Ḣ radical scavenging effect of the resonantly stabilized benzyl and phenoxyl radicals. This negative chemical effect overwhelms the positive thermal effect. However, these differences are negligible if compared to the $T_{ad}$ and $X_H$ of $NH_3$, which are respectively more than 200 K and more than 5000 ppm lower than that of the other two fuels. This confirms that both the thermal and chemical inhibition by $NH_3$ addition play a critical role in the decrease of the $S_L$ of $NH_3$/hydrocarbons mixtures.

Not yet explained is the fact that $S_L$ of toluene is slightly more sensitive to $NH_3$ addition compared to MCH, as shown in Fig. 7. The cause must imply secondary kinetic effects since the analysis reported in Fig. 9 shows that the ratios $T_{ad}^{NH3\text{-}Toluene}/T_{ad}^{NH3\text{-}MCH}$ and $X_H^{NH3\text{-}MCH}/X_H^{NH3\text{-}Toluene}$ keeps constant over a broad range of $NH_3$ mole fraction. First, it is noteworthy that, despite the present kinetic mechanism includes the kinetic interactions among nitrogenous and $C_1$-$C_2$ species, these are found to be irrelevant with respect to the prediction of $S_L$, as no cross-reactions involving nitrogen and carbon radicals show up in the sensitivity analysis, indicating that they do not play a significant role under the conditions of the present flames, in agreement with [48]. It should be noted that co-oxidation reactions between large radical species of toluene and amine radicals leading to substituted $NH_2$-aromatics are overlooked in the present model. In this regard, Altarawneh et al. [105], who explored the $NO_x$ formation from co-combustion of $NH_3$ and benzene, have shown that the inclusion of the aniline sub-mechanism might be required to improve the predictions of $NO_x$ formation in $NH_3$-containing flames. However, because the present mechanism well predicts the effect of $NH_3$ on $S_L$ of toluene, it is unlikely that the interaction between aromatics and amine radicals can be relevant with respect to the prediction of $S_L$.

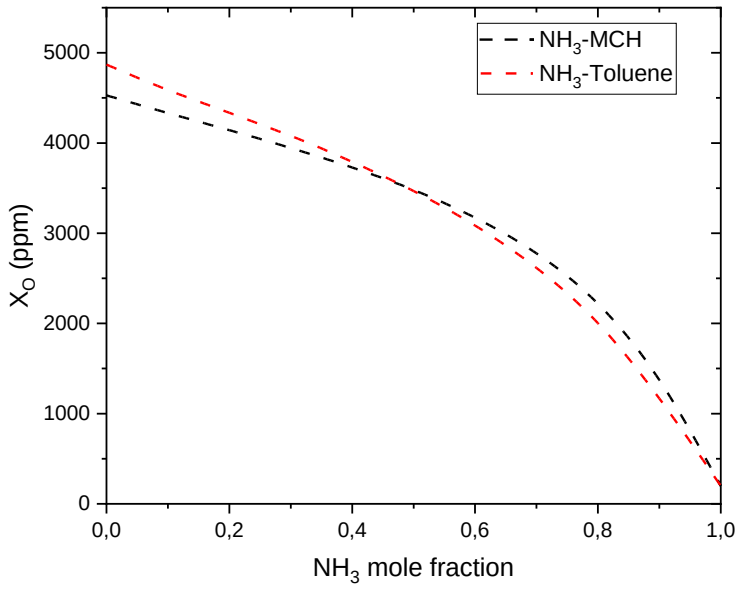


**Figure 10.** Simulated stoichiometric peak $X_O$ versus $NH_3$ mole fraction at $T_g$=338 K and p=1 atm. Black line: MCH/$NH_3$-air mixtures. Red line: toluene/$NH_3$-air mixtures.

Therefore, any disparity in flame structure and kinetic behavior between the MCH and toluene mixtures with $NH_3$ shall be indirect. To further explore this, Fig. 10 plots the impact of $NH_3$ content on the simulated peak mole fraction of Ö radicals in the reaction zone ($X_O$) for the stoichiometric case. From Fig. 10, two considerations must be done. The first is that for pure toluene $X_O$ is higher than that for pure MCH, contrary to Ḣ (Fig. 9) and ȮH radicals. In particular, for pure toluene flames, $X_O$ is comparable to $X_H$. Second, it is seen that the $X_O$ profiles deviate from those of $T_{ad}$ and $X_H$ plotted in Fig. 9. In particular, the $X_O$ trend of $NH_3$/toluene mixtures is steeper than that of $NH_3$/MCH mixtures, corresponding to a stronger Ö radical scavenging effect, which impacts the $S_L$. This deserves further consideration and it is shown in the following discussion to be mostly responsible for the difference in the effect of $NH_3$ on $S_L$ observed both experimentally and numerically.

To further investigate the effect of $NH_3$ on the observed disparity, sensitivity and rate of production analyses were carried out with the proposed mechanism and the simulation results were analyzed focusing attention on the reactions involving the Ö radical. As already seen from Fig. 2, the sensitivity analysis shows that the chain branching reaction $\dot{H}+O_2=\dot{O}H+Ö$ plays a dominant role in all the three fuels flame propagation and it is the main source of Ö. However, the importance of this reaction does not strongly depend on the $NH_3$ content. The radicals generated by this reaction directly contribute to the oxidation of the fuels and small fuel fragments. In fact, it was seen from Fig. 2 that the $S_L$ of both MCH and toluene flames are largely sensitive to the reactions associated with the $C_0$-$C_2$ fuel fragments, whose oxidation kinetics mainly controls the heat release and the overall burning rate. This is indeed a quite general behavior in premixed flames of hydrocarbon fuels, for which the rapid fuel breakdown and the oxidation of fuel fragments can be decoupled [95]. However, unlike the MCH flame, the fuel-specific reactions in the sub-mechanism of toluene also have notable enhancement and inhibition role in the flame propagation kinetics, as identified through the sensitivity analysis. This is mainly related to the stability of the aromatic ring and related products. Among the sensitivity coefficients for various reactions, it is seen that while the $NH_3$ addition has a similar effect on the reactions involving the interaction of Ö with the $H_2$/$C_1$-$C_2$ systems for both fuels, the major difference in the kinetic behavior between $NH_3$/MCH and $NH_3$/toluene blends lies in the reactions involving the toluene immediate oxidation intermediates, which exhibit a strong influence on $S_L$. This can be seen in Fig. 11, which depicts the $S_L$ sensitivity coefficients for the reactions populating the top portion of the sensitivity spectrum, calculated as a function of $NH_3$ mole fraction for binary $NH_3$/toluene mixtures, at $\Phi=1$ and $T_g=338$ K.

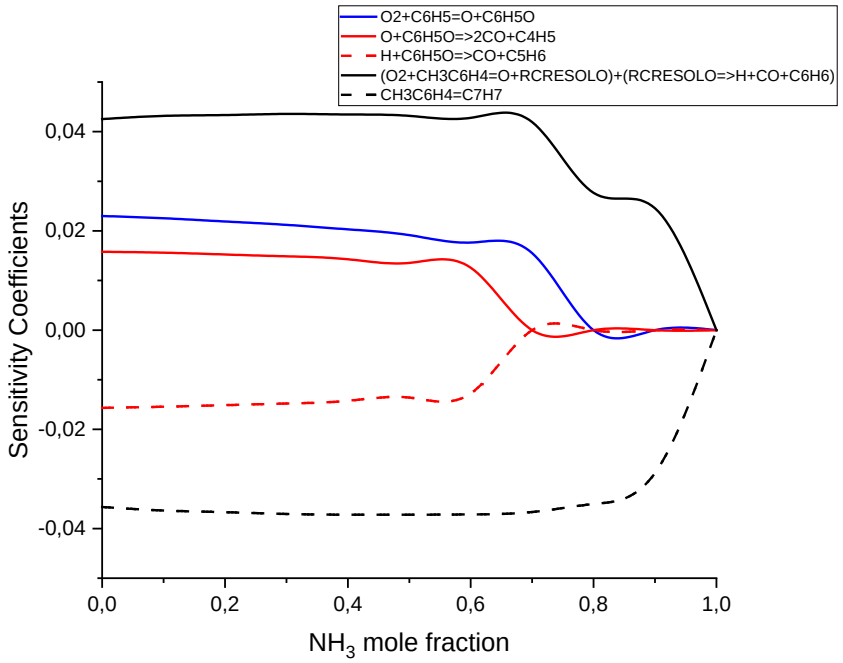


**Figure 11**. $S_L$ sensitivity coefficients of important reactions involving the Ö radical vs. $NH_3$ mole fraction calculated at $\Phi$=1, $T_g$=338 K and p=1 atm for toluene/$NH_3$-air mixtures. Solid lines: reactions with positive $S_L$ sensitivity. Dashed lines: reactions with negative $S_L$ sensitivity.

For MCH, even though the ring opening and subsequent cracking are rather complicated, the influence of fuel-related reactions is certainly much smaller due to the relatively large production of ethylene and vinyl radical, which enhance the overall reactivity of MCH compared to toluene. As already discussed in Section 3.2, during the oxidation of toluene, the benzyl ($C_7H_7$ in Fig. 11) and methyl-phenyl ($CH_3C_6H_4$ in Fig. 11) radical isomers are the primary products from H-abstraction. The benzyl radical is resonantly stabilized, and the benzylic C-H bond is weaker than the phenylic C-H bonds [106]. For these reasons, the reactions of benzyl radical are usually slow and strongly influential in reducing the concentration levels of chain carriers (Fig. 2). As a matter of fact, the isomerization reaction $CH_3C_6H_4=C_7H_7$ (black dashed line in Fig. 11) exhibits a significant negative influence on $S_L$. As an example, the negative sensitivity of such a reaction is

even larger compared to the chain termination reaction Ḣ+$O_2$(+M)=$HO_2$+(M). On the other hand, the addition of the methyl-phenyl radical to $O_2$ leads to the formation of Ö and methyl-phenoxy radicals and the subsequent reactivity of the latter can lead to branching through a decomposition reaction, which constitutes an important contribution to the formation of active Ḣ radicals. This sequence indeed has a very high positive sensitivity and it was reported in Fig. 11 as a single line (black solid) to show that the full sequence is specular with respect to $CH_3C_6H_4$=$C_7H_7$. Though the sensitivity coefficients of these two individual reactions are not as large as those of the most important reaction Ḣ+$O_2$=ȮH+Ö, they are higher compared to $H_2$+Ö=Ḣ+ȮH.

As expected, the $NH_3$ blending modifies the sensitivity coefficients in a nonlinear way. Moreover, it can be seen that for the pure toluene flame the absolute value of the sensitivity of the methyl-phenyl branching sequence is higher than that of the parallel isomerization that forms stable benzyl radicals. However, with increasing $NH_3$, both channels exhibit slightly higher absolute sensitivity coefficients but the relative weight of the isomerization channel increases, showing that the competition between these promoting and inhibiting paths is emphasized. In fact, for an $NH_3$ mole fraction of 0.8, the absolute sensitivity coefficients of the isomerization reaction become higher than that of the branching sequence. This further promotes the depletion of the radicals pool. Additionally, the results of the sensitivity analysis also reveal that another reaction critical to chain termination is the recombination of Ḣ atom with the resonantly stabilized phenoxy radical, Ḣ+$C_6H_5O$=>CO+$C_5H_6$ (red dashed line). It can be seen from Fig. 11 that such a reaction strongly competes with the oxidation of phenoxy by Ö (red solid line), which exhibits specular positive sensitivity coefficients. Phenoxy and Ö radicals are formed via the important oxidation path of phenyl by $O_2$ (blue line). The oxidation of the phenyl radical becomes less important as the $NH_3$ mole fraction increases. This suggests that as soon as Ö atoms become scarce, the competition

discussed above becomes more intense and, for $NH_3$ mole fraction equal to 0.4, $C_6H_5O$+Ḣ prevails over $C_6H_5O$+Ö, thereby further reducing $S_L$. The results of this analysis clearly indicate that the different impact of $NH_3$ chemistry on the $S_L$ of toluene flames compared to that observed for MCH flames should be correlated to the Ö radical scavenging effect of $NH_3$, which further slows down the overall reaction rate by promoting the chain-terminating reactions of the stable benzyl and phenoxyl radicals.

In addition, it was seen from Figs. 5 and 6 that, with the increase of $NH_3$ volume fraction, the percentage decrease in the $S_L$ of both MCH and toluene is slightly higher under rich conditions. Therefore, further sensitivity analyses were carried out and the simulation results were analyzed focusing on the reactions for which the impact of $NH_3$ addition is higher under rich conditions. It was observed that, with increasing Φ, the scavenging effect of $NH_3$, together with the decrease of $T_{ad}$, further promotes the inhibiting effect of chain-terminating reactions in the same way for both MCH and toluene. This can be clearly seen in the case of the methyl recombination reaction $H+CH_3(+M)=CH_4(+M)$. Thus, Fig. 12 depicts the $S_L$ sensitivity coefficients for this reaction calculated as a function of $NH_3$ mole fraction for binary $NH_3$/MCH and $NH_3$/toluene mixtures, at Φ=1 and 1.3. Note that the case of Φ=1 is not reported for $NH_3$/toluene mixtures because such a reaction does not show up in the sensitivity analysis. This channel, which is highly sensitive at Φ>1, slows down the system reactivity because it competes with the methyl oxidation routes. For pure MCH and toluene at Φ=1.3, or for $NH_3$/MCH and $NH_3$/toluene blends at Φ=1, this competition is less stressed.

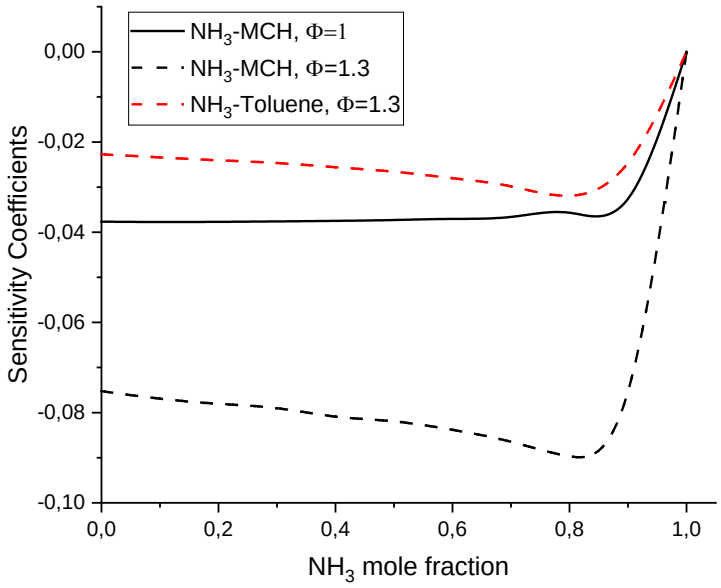


**Figure 12**. $S_L$ sensitivity coefficients of the reaction $H+CH_3(+M)=CH_4(+M)$ vs. $NH_3$ mole fraction calculated at $T_g$=338 K and p=1 atm. Black lines: MCH/$NH_3$-air mixtures. Red line: toluene/$NH_3$-air mixtures. Solid line: Φ=1. Dashed lines: Φ=1.3.

### 5.2 Implications for practical applications

As $S_L$ is a key, but usually unknown, parameter in practical combustion devices, there is also interest to explore if simple mixing rules to estimate $S_L$ can be developed so that the relative proportion of $NH_3$ and hydrocarbons that ensure the successful engine operation can be readily determined. To propose a generalized relationship in order to estimate the $S_L$ of $NH_3$/hydrocarbons mixtures on the basis of those of the individual components, the measured lean (Φ=0.8), stoichiometric, and rich (Φ=1.3) $S_L$ are plotted in Figs. 13a-c versus the quantity of $NH_3$ in mole fraction replacing MCH and toluene in the binary fuel/air mixtures. Also shown in the figure are results from [48] for blends of $NH_3$ with $CH_4$, n-heptane, and iso-octane, obtained under equivalent experimental conditions ($T_g$=338 K and p=1 atm).

(a)

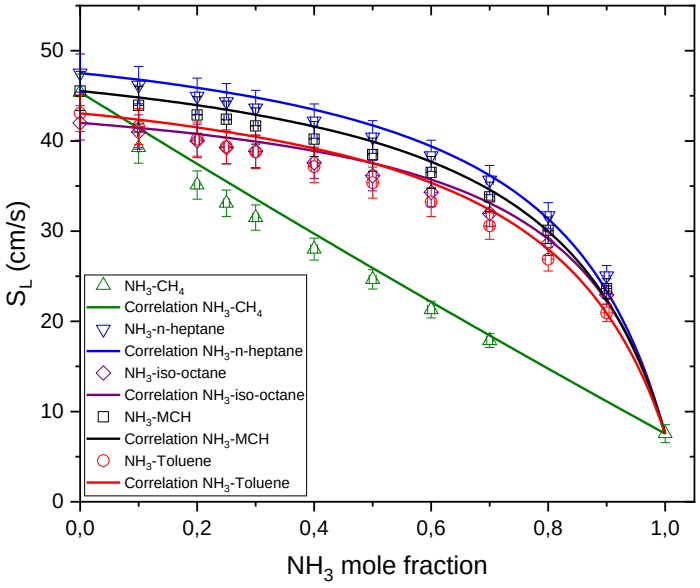
50
40
30
20
10
0
0,0
0,2
0,4
0,6
0,8
1,0
S_L (cm/s)
NH3 mole fraction
NH3-CH4
Correlation NH3-CH4
NH3-n-heptane
Correlation NH3-n-heptane
NH3-iso-octane
Correlation NH3-iso-octane
NH3-MCH
Correlation NH3-MCH
NH3-Toluene
Correlation NH3-Toluene

(b)

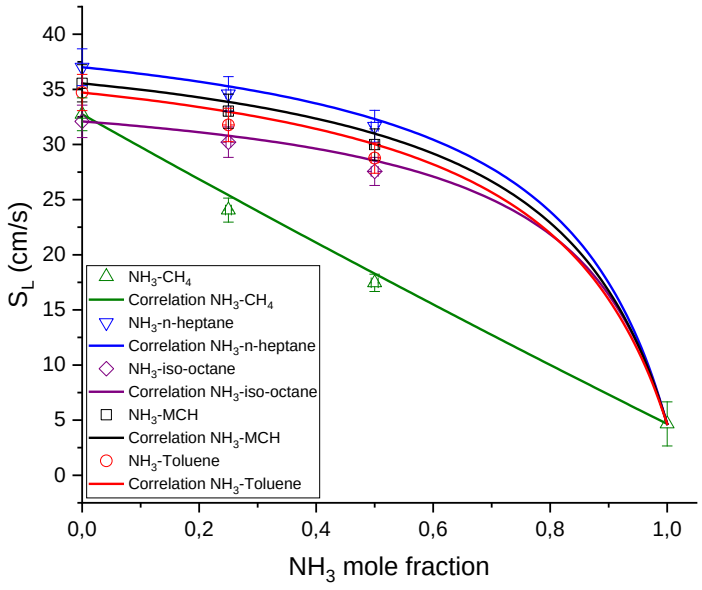
40
35
30
25
20
15
10
5
0
0,0
0,2
0,4
0,6
0,8
1,0
S_L (cm/s)
NH3 mole fraction
NH3-CH4
Correlation NH3-CH4
NH3-n-heptane
Correlation NH3-n-heptane
NH3-iso-octane
Correlation NH3-iso-octane
NH3-MCH
Correlation NH3-MCH
NH3-Toluene
Correlation NH3-Toluene

(c)

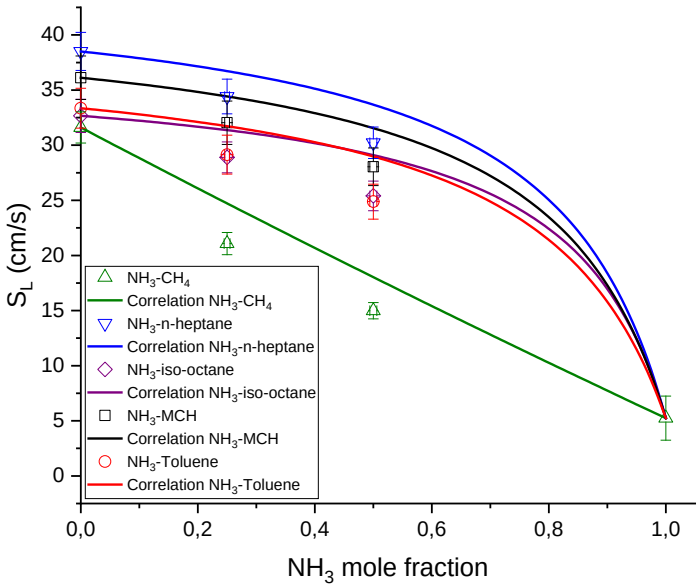


**Figure 13.** Experimental (symbols) and calculated (lines) $S_L$ versus $NH_3$ mole fraction at $T_g$=338 K, p=1 atm, and (a) Φ=1, (b) Φ=0.8, (c) Φ=1.3. Black squares and line: MCH/$NH_3$-air mixtures. Red circles and line: toluene/$NH_3$-air mixtures. Green up triangles and line: $CH_4$/$NH_3$-air mixtures [48]. Blue down triangles and line: n-heptane/$NH_3$-air mixtures [48]. Purple diamonds and line: iso-octane/$NH_3$-air mixtures [48]. The values of $S_L$ for pure $NH_3$ are from [41].

As already observed in Fig. 7, the evolution is nonlinear and antagonist with the mole fraction of $NH_3$. However, our previous study [48] suggested that the $S_L$ for flames of $NH_3$ in combination with methane, n-heptane, and iso-octane has a quasi-linear correlation with the $NH_3$ mass fraction in the fuel blend, instead of mole fraction. Thus, it is interesting to test if the relationship between the $S_L$ of any hydrocarbon class, including naphtenes and aromatics, and the $NH_3$ ratio can be expressed as $(1-Y_{NH3})(S_L^0)+(Y_{NH3})(S_L^{NH3})$, where $S_L^0$ is the value at zero $NH_3$ addition and $Y_{NH3}$ is the $NH_3$ mass fraction. The lines in Fig. 13 show the relationship approximated by this equation. A similar plot as a function of the $NH_3$ mass fraction is reported in Fig. S34 of the Supplementary Material. It can be observed that the $S_L$ values calculated in this simple way are within the uncertainty of the measured ones for most of the examined mixtures. Thus, it can be concluded

that the addition of $NH_3$ similarly affects the $S_L$ of hydrocarbons, independent of the carbon number ($C_1$-$C_8$) and fuel class (linear, branched, and cyclic alkanes, aromatics). The reason for this similarity is that, as explained above, the influence of $NH_3$ on $S_L$ of hydrocarbons is mostly dominated by flame temperature and activation energy, with little kinetic coupling. This finding can also help to develop reduced mechanisms for surrogate fuels to implement in CFD modeling. However, it must be noted that the proposed mixing rule is less valid under rich conditions, or when applied to the $S_L$ of binary mixtures of $NH_3$ with $CH_4$ or toluene, independent on Φ. The reason is that for these mixtures the addition of $NH_3$ implies secondary kinetic effects as explained in the previous section. Regarding $NH_3$/$CH_4$ blends, it was observed in [48] that the higher impact of $NH_3$ addition on $S_L$ of $CH_4$ compared to heavy hydrocarbons is due to a decrease in the hydrogen concentration in the flame zone, which induces an inhibiting effect only in the case of $CH_4$. This was considered as a combined chemical and transport effect because of the high reactivity and diffusivity of hydrogen.

Therefore, it is clear that this correlation, despite more convenient, is only approximate and such deviations do need to be kept in mind when quantitative information concerning fuel similarities or dissimilarities at specific operating points is needed. In these cases, predictions from detailed kinetic models are more valuable. Notwithstanding, the fact that this predictive relationship can be applied equally well to the $S_L$ computed for all the mixtures further points out that the mutual interference between the components of a binary blend of $NH_3$ with hydrocarbons, when present, has only a minor effect with respect to the whole $NH_3$ contribution to $S_L$, at least under the conditions explored in the present and previous work [48]. Further confirmations at higher temperatures and pressures would be worthwhile in order to deduce whether the above correlation can be used to provide support for practical engines and gas turbines design and operation.

## 6. Conclusions

This work focuses on a combined experimental and modeling investigation on the influence of $NH_3$ on the propagation of MCH and toluene laminar flames. These hydrocarbons are typical of the component classes found in actual internal combustion engines and aviation fuels. The overall objective was to provide experimental data and a chemical kinetic model for blends of $NH_3$ with large hydrocarbons, which would be relevant to examine the optimal operation in realistic applications such as internal combustion engines. Specifically, an extensive experimental database on $S_L$ for $NH_3$/MCH/air and $NH_3$/toluene/air was acquired at atmospheric pressure and 338 K, for equivalence ratios ranging from 0.7 to 1.3, and $NH_3$ blending levels in the fuel from 0% to 90%, using the heat flux method. About 60 new data points are presented, that significantly enrich the literature data. A comprehensive chemical kinetic model has been developed based on the existing CRECK chemical kinetic mechanism where the high temperature combustion chemistry was improved with minor adjustments, paying attention to the proper description of the consumption of methylcyclohexane, toluene, and methyl-phenoxy radical. The main findings are summarized as follows:

1. The present results on pure MCH/air and pure toluene/air flames are in reasonably close agreement with previous measurements from the literature obtained with the same method, although small discrepancies are observed under rich conditions.

2. A monotonic decrease in $S_L$ with increasing $NH_3$ content is observed. The results show that both the equivalence ratio and the $NH_3$ fraction have an important impact on the $S_L$ of $NH_3$/hydrocarbon fuel blends. In particular, when the equivalence ratio is held constant, the $S_L$ decreases nonlinearly with increasing the $NH_3$ mole fraction, but this influence becomes quasi-linear when the $NH_3$

concentration is considered on a mass basis. This behavior is qualitatively consistent with previous investigations for blends of $NH_3$ with alkanes. In addition, $NH_3$ has a slightly higher effect on the $S_L$ of toluene compared to MCH.

3. A comparison of the present measurements with detailed chemical kinetic simulations using the current refined reaction mechanism showed an overall good agreement over the whole range of investigation. On the other hand, the results presented herein showed that additional systematic theoretical studies for reaction classes concerning aromatic compounds and oxygenated aromatic intermediates are still required to improve the prediction of $S_L$ in the case of toluene/air flames.

4. With the refined model, detailed analyses have also been conducted to provide fundamental insights into the physical and chemical blending effects of $NH_3$ with different classes of compounds that cause the $S_L$ variation in binary mixtures. It was found that, similar to alkanes, the synergistic thermal and chemical effects of $NH_3$ play a predominant role in the decrease of the $S_L$ for both $NH_3$/MCH and $NH_3$/toluene mixtures. The thermal effect is due to the decrease of the adiabatic flame temperature with increasing the $NH_3$ fraction, while the flame structure analyses revealed that the decrease in chemical reactivity is mainly caused by the reduction of Ḣ, Ö, and ȮH concentrations in the flame. The observed higher inhibition of $NH_3$ on toluene flames compared to MCH is most likely referable to their different molecular structures. In particular, the Ö radical scavenging effect of $NH_3$ further slows down the overall reaction rate by exerting a promoting effect on the chain-terminating reactions of the stable benzyl and phenoxyl radicals. The elucidation of fuel structure effects was the primary reason for the selection of MCH and toluene in this work.

5. A mass fraction-based mixing rule was also proposed and tested against the data collected in the present study and from the literature. This mixing rule, although simple, was shown to be

predictive for binary blends of $NH_3$ with methane and several hydrocarbons typically used to formulate surrogates for practical fuels, suggesting that the kinetic coupling between $NH_3$ and toluene, despite present, is limited.

**Funding**

This work was supported by the Swedish Energy Agency via the Centre for Combustion Science and Technology [Project KC-CECOST 22538-4], Sweden.

**References**

[1] A. Valera-Medina, H. Xiao, M. Owen-Jones, W.I.F. David, P.J. Bowen, Ammonia for power, Prog. Energy Combust. Sci. 69 (2018) 63-102.

[2] C.S. Mørch, A. Bjerre, M.P. Gøttrup, S.C. Sorenson, J. Schramm, Ammonia/hydrogen mixtures in an SI-engine: Engine performance and analysis of a proposed fuel system, Fuel 90 (2011) 854-864.

[3] S.S. Gill, G.S. Chatha, A. Tsolakis, S.E. Golunski, A.P.E. York, Assessing the effects of partially decarbonising a diesel engine by co-fuelling with dissociated ammonia, Int. J. Hydrogen Energy 37 (2012) 6074-6083.

[4] F.R. Westlye, A. Ivarsson, J. Schramm, Experimental investigation of nitrogen based emissions from an ammonia fueled SI-engine, Fuel 111 (2013) 239-247.

[5] S. Frigo, R. Gentili, Analysis of the behaviour of a 4-stroke Si engine fuelled with ammonia and hydrogen, Int. J. Hydrogen Energy 38 (2013) 1607-1615.

[6] K. Ryu, G.E. Zacharakis-Jutz, S.-C. Kong, Effects of gaseous ammonia direct injection on performance characteristics of a spark-ignition engine, Appl. Energy 116 (2014) 206-215.

[7] A. Valera-Medina, S. Morris, J. Runyon, D.G. Pugh, R. Marsh, P. Beasley, T. Hughes, Ammonia, methane and hydrogen for gas turbines, Energy Procedia 75 (2015) 118-123.

[8] A. Valera-Medina, D.G. Pugh, P. Marsh, G. Bulat, P. Bowen, Preliminary study on lean premixed combustion of ammonia-hydrogen for swirling gas turbine combustors, Int. J. Hydrogen Energy 42 (2017) 24495-24503.

[9] A. Valera-Medina, M. Gutesa, H. Xiao, D. Pugh, A. Giles, B. Goktepe, R. Marsh, P. Bowen, Premixed ammonia/hydrogen swirl combustion under rich fuel conditions for gas turbines operation, Int. J. Hydrogen Energy 44 (2019) 8615-8626.

[10] M. Pochet, I. Truedsson, F. Foucher, H. Jeanmart, F. Contino, Ammonia-hydrogen blends in Homogeneous-Charge Compression-Ignition engine, SAE Tech. Pap. Ser. (2017) DOI: 10.4271/2017-24-0087.

[11] M. Pochet, H. Jeanmart, F. Contino, A 22:1 compression ratio ammonia-hydrogen HCCI engine: combustion, load, and emission performances, Front. Mech. Eng. 6, 43 (2020).

[12] D. Pugh, P. Bowen, A. Valera-Medina, A. Giles, J. Runyon, R. Marsh, Influence of steam addition and elevated ambient conditions on $NO_x$ reduction in a staged premixed swirling $NH_3/H_2$ flame, Proc. Combust. Inst. 37 (2019) 5401-5409.

[13] C. Lhuillier, P. Brequigny, F. Contino, C. Rousselle, Performance and emissions of an ammonia-fueled SI engine with hydrogen enrichment, SAE Tech. Pap. Ser. (2019) DOI: 10.4271/2019-24-0137.

[14] C. Lhuillier, P. Brequigny, F. Contino, C. Rousselle, Combustion characteristics of ammonia in a modern Spark-Ignition engine, SAE Tech. Pap. Ser. (2019) DOI: 10.4271/2019-24-0237.

[15] C. Lhuillier, P. Brequigny, F. Contino, C. Mounaïm-Rousselle, Experimental study on ammonia/hydrogen/air combustion in spark ignition engine conditions, Fuel 269 (2020) 117448.

[16] C. Lhuillier, P. Brequigny, F. Contino, C. Mounaïm-Rousselle, Experimental investigation on ammonia combustion behavior in a spark-ignition engine by means of laminar and turbulent expanding flames, Proc. Combust. Inst. 38 (2021) 5859-5868.

[17] A. Valera-Medina, R. Marsh, J. Runyon, D. Pugh, P. Beasley, T. Hughes, P. Bowen, Ammonia-methane combustion in tangential swirl burners for gas turbine power generation, Appl. Energy 185 (2017) 1362-1371.

[18] H. Xiao, A. Valera-Medina, R. Marsh, P.J. Bowen, Numerical study assessing various ammonia/methane reaction models for use under gas turbine conditions, Fuel 196 (2017) 344-351.

[19] O. Kurata, N. Iki, T. Matsunuma, T. Inoue, T. Tsujimura, H. Furutani, H. Kobayashi, A. Hayakawa, Performances and emission characteristics of $NH_3$-air and $NH_3$-$CH_4$-air combustion gas-turbine power generations, Proc. Combust. Inst. 36 (2017) 3351-3359.

[20] A.J. Reiter, S.-C. Kong, Demonstration of Compression-Ignition engine combustion using ammonia in reducing greenhouse gas emissions, Energy Fuels 22 (2008) 2963-2971.

[21] A.J. Reiter, S.-C. Kong, Combustion and emissions characteristics of compression-ignition engine using dual ammonia-diesel fuel, Fuel 90 (2011) 87-97.

[22] A. Boretti, Novel dual fuel diesel-ammonia combustion system in advanced TDI engines, Int. J. Hydrogen Energy 42 (2017) 7071-7076.

[23] Z. Şahin, İ.Z. Akcanca, O. Durgun, Experimental investigation of the effects of ammonia solution ($NH_3OH$) on engine performance and exhaust emissions of a small diesel engine, Fuel 214 (2018) 330-341.

[24] C.W. Gross, S.-C. Kong, Performance characteristics of a compression-ignition engine using direct-injection ammonia-DME mixtures, Fuel 103 (2013) 1069-1079.

[25] K. Ryu, G.E. Zacharakis-Jutz, S.-C. Kong, Performance characteristics of compression-ignition engine using high concentration of ammonia mixed with dimethyl ether, Appl. Energy 113 (2014) 488-499.

[26] S.M. Grannell, D.N. Assanis, S.V. Bohac, D.E. Gillespie, The fuel mix limits and efficiency of a stoichiometric, ammonia, and gasoline dual fueled Spark Ignition engine, J. Eng. Gas Turbines Power 130 (2008) No. 042802.

[27] M. Koike, H. Miyagawa, T. Suzuoki, K. Ogasawara, Ammonia as a hydrogen energy carrier and its application to internal combustion engines, Sustainable Veh. Technol. (2012) 61-70.

[28] A. Yapicioglu, I. Dincer, Performance assesment of hydrogen and ammonia combustion with various fuels for power generators, Int. J. Hydrogen Energy 43 (2018) 21037-21048.

[29] S.O. Haputhanthri, Ammonia gasoline fuel blends: feasibility study of commercially available emulsifiers and effects on stability and engine performance, SAE Tech. Pap. Ser. (2014) DOI: 10.4271/2014-01-2759.

[30] P.F. Henshaw, T. D'Andrea, K.R.C. Mann, D.S.-K. Ting, Premixed ammonia-methane-air combustion, Combust. Sci. Technol. 177 (2005) 2151-2170.

[31] K. Takizawa, A. Takahashi, K. Tokuhashi, S. Kondo, A. Sekiya, Burning velocity measurements of nitrogen-containing compounds, J. Hazard. Mater. 155 (2008) 144-152.

[32] J.H. Lee, J.H. Kim, J.H. Park, O.C. Kwon, Studies on properties of laminar premixed hydrogen-added ammonia/air flames for hydrogen production, Int. J. Hydrogen Energy 35 (2010) 1054-1064.

[33] P. Kumar, T.R. Meyer, Experimental and modeling study of chemical-kinetics mechanisms for $H_2$-$NH_3$-air mixtures in laminar premixed jet flames, Fuel 108 (2013) 166-176.

[34] A. Hayakawa, T. Goto, R. Mimoto, Y. Arakawa, T. Kudo, H. Kobayashi, Laminar burning velocity and Markstein length of ammonia/air premixed flames at various pressures, Fuel 159 (2015) 98-106.

[35] A. Ichikawa, A. Hayakawa, Y. Kitagawa, K.D.K.A. Somarathne, T. Kudo, H. Kobayashi, Laminar burning velocity and Markstein length of ammonia/hydrogen/air premixed flames at elevated pressures, Int. J. Hydrogen Energy 40 (2015) 9570-9578.

[36] E.C. Okafor, Y. Naito, S. Colson, A. Ichikawa, T. Kudo, A. Hayakawa, H. Kobayashi, Experimental and numerical study of the laminar burning velocity of $CH_4$-$NH_3$-air premixed flames, Combust. Flame 187 (2018) 185-198.

[37] B. Mei, X. Zhang, S. Ma, M. Cui, H. Guo, Z. Cao, Y. Li, Experimental and kinetic modeling investigation on the laminar flame propagation of ammonia under oxygen enrichment and elevated pressure conditions, Combust. Flame 210 (2019) 236-246.

[38] Q. Liu, X. Chen, J. Huang, Y. Shen, Y. Zhang, Z. Liu, The characteristics of flame propagation in ammonia/oxygen mixtures, J. Hazard. Mater. 363 (2019) 187-196.

[39] X. Han, Z. Wang, M. Costa, Z. Sun, Y. He, K. Cen, Experimental and kinetic modeling study of laminar burning velocities of $NH_3$/air, $NH_3$/$H_2$/air, $NH_3$/CO/air and $NH_3$/$CH_4$/air premixed flames, Combust. Flame 206 (2019) 214-226.

[40] E.C. Okafor, Y. Naito, S. Colson, A. Ichikawa, T. Kudo, A. Hayakawa, H. Kobayashi, Measurement and modelling of the laminar burning velocity of methane-ammonia-air flames at high pressures using a reduced reaction mechanism, Combust. Flame 204 (2019) 162-175.

[41] X. Han, Z. Wang, Y. He, Y. Liu, Y. Zhu, A.A. Konnov, The temperature dependence of the laminar burning velocity and superadiabatic flame temperature phenomenon for $NH_3$/air flames, Combust. Flame 217 (2020) 314-320.

[42] X. Han, Z. Wang, Y. He, Y. Zhu, K. Cen, Experimental and kinetic modeling study of laminar burning velocities of NH3/syngas/air premixed flames, Combust. Flame 213 (2020) 1-13.

[43] C. Lhuillier, P. Brequigny, N. Lamoureux, F. Contino, C. Mounaïm-Rousselle, Experimental investigation on laminar burning velocities of ammonia/hydrogen/air mixtures at elevated temperatures, Fuel 263 (2020) 116653.

[44] H. Lesmana, M. Zhu, Z. Zhang, J. Gao, J. Wu, D. Zhang, Experimental and kinetic modelling studies of laminar flame speed in mixtures of partially dissociated $NH_3$ in air, Fuel 278 (2020) 118428.

[45] S. Wang, Z. Wang, A.M. Elbaz, X. Han, Y. He, M. Costa, A.A. Konnov, W.L. Roberts, Experimental study and kinetic analysis of the laminar burning velocity of $NH_3$/syngas/air, $NH_3$/CO/air and $NH_3$/$H_2$/air premixed flames at elevated pressures, Combust. Flame 221 (2020) 270-287.

[46] K.P. Shrestha, C. Lhuillier, A.A. Barbosa, P. Brequigny, F. Contino, C. Mounaïm-Rousselle, L. Seidel, F. Mauss, An experimental and modeling study of ammonia with enriched oxygen content and ammonia/hydrogen laminar flame speed at elevated pressure and temperature, Proc. Combust. Inst. 38 (2021) 2163-2174.

[47] X. Han, M. Lubrano Lavadera, A.A. Konnov, An experimental and kinetic modeling study on the laminar burning velocity of $NH_3$+$N_2O$+air flames, Combust. Flame 228 (2021) 13-28.

[48] M. Lubrano Lavadera, X. Han, A.A. Konnov, Comparative effect of ammonia addition on the laminar burning velocities of methane, n-heptane, and iso-octane, Energy Fuels 35 (2021) 7156-7168.

[49] W.J. Pitz, N.P. Cernansky, F.L. Dryer, F.N. Egolfopoulos, J.T. Farrell, D.G. Friend, H. Pitsch, Development of an experimental database and chemical kinetic models for surrogate gasoline fuels, SAE Trans. 116 (2007) 195-216.

[50] J.T. Farrell, N.P. Cernansky, F.L. Dryer, C.K. Law, D.G. Friend, C.A. Hergart, R.M. McDavid, A.K. Patel, C.J. Mueller, H. Pitsch, Development of an experimental database and kinetic models for surrogate diesel fuels, SAE Tech. Pap. Ser. (2007) DOI: 10.4271/2007-01-0201.

[51] V.A. Alekseev, J.D. Naucler, M. Christensen, E.J. Nilsson, E.N. Volkov, L.P.H. de Goey, A.A. Konnov, Experimental uncertainties of the heat flux method for measuring burning velocities, Combust. Sci. Technol. 188 (2016) 853-894.

[52] R.T.E. Hermanns, Laminar burning velocities of methane-hydrogen-air mixtures. Ph.D. Thesis, Eindhoven University of Technology, Eindhoven, Netherlands, 2007.

[53] http://creckmodeling.chem.polimi.it/menu-kinetics/menu-kinetics-detailed-mechanisms

[54] E. Ranzi, A. Frassoldati, A. Stagni, M. Pelucchi, A. Cuoci, T. Faravelli, Reduced kinetic schemes of complex reaction systems: fossil and biomass-derived transportation fuels, Int. J. Chem. Kinet. 46 (2014) 512-542.

[55] Y. Song, L. Marrodán, N. Vin, O. Herbinet, E. Assaf, C. Fittschen, A. Stagni, T. Faravelli, M.U. Alzueta, F. Battin-Leclerc, The sensitizing effects of $NO_2$ and NO on methane low temperature oxidation in a jet stirred reactor, Proc. Combust. Inst. 37 (2019) 667-675.

[56] A. Stagni, C. Cavallotti, S. Arunthanayothin, Y. Song, O. Herbinet, F. Battin-Leclerc, T. Faravelli, An experimental, theoretical and kinetic-modeling study of the gas-phase oxidation of ammonia, React. Chem. Eng. 5 (2020) 696-711.

[57] C. Saggese, S. Ferrario, J. Camacho, A. Cuoci, A. Frassoldati, E. Ranzi, H. Wang, T. Faravelli, Kinetic modeling of particle size distribution of soot in a premixed burner-stabilized stagnation ethylene flame, Combust. Flame 162 (2015) 3356-3369.

[58] W. Pejpichestakul, A. Cuoci, A. Frassoldati, M. Pelucchi, A. Parente, T. Faravelli, Buoyancy effect in sooting laminar premixed ethylene flame, Combust. Flame 205 (2019) 135-146.

[59] W. Pejpichestakul, A. Frassoldati, A. Parente, T. Faravelli, Soot modeling of ethylene counterflow diffusion flames, Combust. Sci. Technol. 191 (2019) 1473-1483.

[60] W.K. Metcalfe, S.M. Burke, S.S. Ahmed, H.J. Curran, A hierarchical and comparative kinetic modeling study of $C_1$-$C_2$ hydrocarbon and oxygenated fuels, Int. J. Chem. Kinet. 45 (2013) 638-675.

[61] S.M. Burke, U. Burke, R. Mc Donagh, O. Mathieu, I. Osorio, C. Keesee, A. Morones, E.L. Petersen, W. Wang, T.A. DeVerter, M.A. Oehlschlaeger, B. Rhodes, R.K. Hanson, D.F. Davidson, B.W. Weber, C.-J. Sung, J. Santner, Y. Ju, F.M. Haas, F.L. Dryer, E.N. Volkov, E.J.K. Nilsson, A.A. Konnov, M. Alrefae, F. Khaled, A. Farooq, P. Dirrenberger, P.-A. Glaude, F. Battin-Leclerc, H.J. Curran, An experimental and modeling study of propene oxidation. Part 2: Ignition delay time and flame speed measurements, Combust. Flame 162 (2015) 296-314.

[62] G. Bagheri, E. Ranzi, M. Pelucchi, A. Parente, A. Frassoldati, T. Faravelli, Comprehensive kinetic study of combustion technologies for low environmental impact: MILD and OXY-fuel combustion of methane, Combust. Flame 212 (2020) 142-155.

[63] W. Pejpichestakul, E. Ranzi, M. Pelucchi, A. Frassoldati, A. Cuoci, A. Parente, T. Faravelli, Examination of a soot model in premixed laminar flames at fuel-rich conditions, Proc. Combust. Inst. 37 (2019) 1013-1021.

[64] M. Pelucchi, C. Cavallotti, A. Cuoci, T. Faravelli, A. Frassoldati, E. Ranzi, Detailed kinetics of substituted phenolic species in pyrolysis bio-oils, React. Chem. Eng. 4 (2019) 490-506.

[65] L. Pratali Maffei, T. Faravelli, C. Cavallotti, M. Pelucchi, Electronic structure-based rate rules for Ḣ *ipso* addition-elimination reactions on mono-aromatic hydrocarbons with single and double $OH/CH_3/OCH_3/CHO/C_2H_5$ substituents: a systematic theoretical investigation, Phys. Chem. Chem. Phys. 22 (2020) 20368-20387.

[66] L. Pratali Maffei, M. Pelucchi, T. Faravelli, C. Cavallotti, Theoretical study of sensitive reactions in phenol decomposition, React. Chem. Eng. 5 (2020) 452-472.

[67] G. Mairinger, A. Frassoldati, A. Cuoci, M. Pelucchi, E. Pucher, K. Seshadri, Experimental and computational investigation of autoignition of jet fuels and surrogates in nonpremixed flows at elevated pressures, Proc. Combust. Inst. 37 (2019) 1605-1614.

[68] M. Pelucchi, C. Cavallotti, T. Faravelli, S.J. Klippenstein, H-Abstraction reactions by OH, $HO_2$, O, $O_2$ and benzyl radical addition to $O_2$ and their implications for kinetic modelling of toluene oxidation, Phys. Chem. Chem. Phys. 20 (2018) 10607-10627.

[69] H.-P.S. Shen, J. Vanderover, M.A. Oehlschlaeger, A shock tube study of the auto-ignition of toluene/air mixtures at high pressures, Proc. Combust. Inst. 32 (2009) 165-172.

[70] W. Yuan, Y. Li, P. Dagaut, J. Yang, F. Qi, Investigation on the pyrolysis and oxidation of toluene over a wide range conditions. II. A comprehensive kinetic modeling study, Combust. Flame 162 (2015) 22-40.

[71] Y. Zhang, K.P. Somers, M. Mehl, W.J. Pitz, R.F. Cracknell, H.J. Curran, Probing the antagonistic effect of toluene as a component in surrogate fuel models at low temperatures and high pressures. A case study of toluene/dimethyl ether mixtures, Proc. Combust. Inst. 36 (2017) 413-421.

[72] A. Burcat, C. Snyder, T. Brabbs, Ignition delay times of benzene and toluene with oxygen in argon mixtures, NASA Tech. Memo. (1986) 87312.

[73] K.M. Pamidimukkala, R.D. Kern, M.R. Patel, H.C. Wei, J.H. Kiefer, High-temperature pyrolysis of toluene, J. Phys. Chem. 91 (1987) 2148-2154.

[74] M.B. Colket, D.J. Seery, Reaction mechanisms for toluene pyrolysis, Symp. (Int.) Combust. 25 (1994) 883-891.

[75] R. Sivaramakrishnan, R.S. Tranter, K. Brezinsky, High pressure pyrolysis of toluene. 1. Experiments and modeling of toluene decomposition, J. Phys. Chem. 110 (2006) 9388-9399.

[76] R. Bounaceur, I. Da Costa, R. Fournet, F. Billaud, F. Battin-Leclerc, Experimental and modeling study of the oxidation of toluene, Int. J. Chem. Kinet. 37 (2005) 25-49.

[77] P. Dagaut, G. Pengloan, A. Ristori, Oxidation, ignition and combustion of toluene: experimental and detailed chemical kinetic modeling, Phys. Chem. Chem. Phys. 4 (2002) 1846-1854.

[78] G. Pengloan, P. Dagaut, N. Djebaili-Chaumeix, C.E. Paillard, M. Cathonnet, Colloque combustion propre, Combustion Institute, French Section (2001), 9.

[79] V. Vasudevan, D.F. Davidson, R.K. Hanson, Shock tube measurements of toluene ignition times and OH concentration time histories, Proc. Combust. Inst. 30 (2005) 1155-1163.

[80] R. Sivaramakrishnan, R.S. Tranter, K. Brezinsky, High pressure pyrolysis of toluene. 2. Modeling benzyl decomposition and formation of soot precursors, J. Phys. Chem. A 110 (2006) 9400-9404.

[81] K. Narayanaswamy, G. Blanquart, H. Pitsch, A consistent chemical mechanism for oxidation of substituted aromatic species, Combust. Flame 157 (2010) 1879-1898.

[82] W.K. Metcalfe, S. Dooley, F.L. Dryer, Comprehensive detailed chemical kinetic modeling study of toluene oxidation, Energy Fuels 25 (2011) 4915-4936.

[83] J. Herzler, M. Fikri, K. Hitzbleck, R. Starke, C. Schulz, P. Roth, G.T. Kalghatgi, Shock-tube study of the autoignition of n-heptane/toluene/air mixtures at intermediate temperatures and high pressures, Combust. Flame 149 (2007) 25-31.

[84] R. Sivaramakrishnan, R.S. Tranter, K. Brezinsky, High-pressure, high-temperature oxidation of toluene, Combust. Flame 139 (2004) 340-350.

[85] P. Dirrenberger, P.A. Glaude, R. Bounaceur, H. Le Gall, A. Pires da Cruz, A.A. Konnov, F. Battin-Leclerc, Laminar burning velocity of gasolines with addition of ethanol, Fuel 115 (2014) 162-169.

[86] G. Wang, Y. Li, W. Yuan, Z. Zhou, Y. Wang, Z. Wang, Investigation on laminar burning velocities of benzene, toluene and ethylbenzene up to 20 atm, Combust. Flame 184 (2017) 312-323.

[87] B.W. Weber, W.J. Pitz, M. Mehl, E.J. Silke, A.C. Davis, C.-J. Sung, Experiments and modeling of the autoignition of methylcyclohexane at high pressure, Combust. Flame 161 (2014) 1972-1983.

[88] T. Bissoonauth, Z. Wang, S.Y. Mohamed, J.-y. Wang, B. Chen, A. Rodriguez, O. Frottier, X. Zhang, Y. Zhang, C. Cao, J. Yang, O. Herbinet, F. Battin-Leclerc, S.M. Sarathy, Methylcyclohexane pyrolysis and oxidation in a jet-stirred reactor, Proc. Combust. Inst. 37 (2019) 409-417.

[89] J.P. Orme, H.J. Curran, J.M. Simmie, Experimental and modeling study of methyl cyclohexane pyrolysis and oxidation, J. Phys. Chem. A 110 (2006) 114-131.

[90] S.S. Vasu, D.F. Davidson, Z. Hong, R.K. Hanson, Shock tube study of methylcyclohexane ignition over a wide range of pressure and temperature, Energy Fuels 23 (2009) 175-185.

[91] J. Vanderover, M.A. Oehlschlaeger, Ignition time measurements for methylcyclohexane- and ethylcyclohexane-air mixtures at elevated pressures, Int. J. Chem. Kinet. 41 (2009) 82-91.

[92] F. Wu, A.P. Kelley, C.K. Law, Laminar flame speeds of cyclohexane and mono-alkylated cyclohexanes at elevated pressures, Combust. Flame 159 (2012) 1417-1425.

[93] C. Ji, E. Dames, B. Sirjean, H. Wang, F.N. Egolfopoulos, An experimental and modeling study of the propagation of cyclohexane and mono-alkylated cyclohexane flames, Proc. Combust. Inst. 33 (2011) 971-978.

[94] M. Pelucchi, A. Stagni, T. Faravelli, Addressing the complexity of combustion kinetics: Data management and automatic model validation, in: T. Faravelli, F. Manenti, E. Ranzi (Eds.), Computer Aided Chemical Engineering Vol. 45, Elsevier, 2019, pp. 763-798.

[95] E. Ranzi, A. Frassoldati, R. Grana, A. Cuoci, T. Faravelli, A.P. Kelley, C.K. Law, Hierarchical and comparative kinetic modeling of laminar flame speeds of hydrocarbon and oxygenated fuels, Prog. Energy Combust. Sci. 38 (2012) 468-501.

[96] Z. Wang, L. Ye, W. Yuan, L. Zhang, Y. Wang, Z. Cheng, F. Zhang, F. Qi, Experimental and kinetic modeling study on methylcyclohexane pyrolysis and combustion, Combust. Flame 161 (2014) 84-100.

[97] S.-H. Li, J.-J. Guo, R. Li, F. Wang, X.-Y. Li, Theoretical prediction of rate constants for hydrogen abstraction by OH, H, O, $CH_3$, and $HO_2$ radicals from toluene, J. Phys. Chem. A 120 (2016) 3424-3432.

[98] S.W. Wagnon, S. Thion, E.J.K. Nilsson, M. Mehl, Z. Serinyel, K. Zhang, P. Dagaut, A.A. Konnov, G. Dayma, W.J. Pitz, Experimental and modeling studies of a biofuel surrogate

compound: laminar burning velocities and jet-stirred reactor measurements of anisole, Combust. Flame 189 (2018) 325-336.

[99] J.M. Simmie, K.P. Somers, Benchmarking compound methods (CBS-QB3, CBS-APNO, G3, G4, W1BD) against the active thermochemical tables: a litmus test for cost-effective molecular formation enthalpies, J. Phys. Chem. A 119 (2015) 7235-7246.

[100] G. da Silva, C.-C. Chen, J.W. Bozzelli, Toluene combustion: reaction paths, thermochemical properties, and kinetic analysis for the methylphenyl radical + $O_2$ reaction, J. Phys. Chem. A 111 (2007) 8663-8676.

[101] S.S. Matveev, D.V. Idrisov, S.G. Matveev, A.A. Konnov, Laminar burning velocities of surrogate components blended with ethanol, Combust. Flame 209 (2019) 389-393.

[102] L. Sileghem, V.A. Alekseev, J. Vancoillie, K.M. Van Geem, E.J.K. Nilsson, S. Verhelst, A.A. Konnov, Laminar burning velocity of gasoline and the gasoline surrogate components iso-octane, n-heptane and toluene, Fuel 112 (2013) 355-365.

[103] Y. Zhang, Q. Li, H. Liu, Z. Yan, Z. Huang, Comparative study on the laminar flame speeds of methylcyclohexane-methanol and toluene-methanol blends at elevated temperatures, Fuel 245 (2019) 534-543.

[104] B.-J. Zhong, H.-S. Peng, D. Zheng, The effect of different class of hydrocarbons on laminar flame speeds of three $C_7$ fuels, Fuel 225 (2018) 225-229.

[105] I.S. Altarawneh, M. Altarawneh, S.E. Rawadieh, M.H. Almatarneh, A. Shiroudi, A.M. El-Nahas, Updated yields of nitrogenated species in flames of ammonia/benzene via introducing an aniline sub-mechanism, Combust. Flame 228 (2021) 433-442.

[106] C. Ji, E. Dames, H. Wang, F.N. Egolfopoulos, Propagation and extinction of benzene and alkylated benzene flames, Combust. Flame 159 (2012) 1070-1081.